Stability-constrained Optimal Power Flow for AC Microgrids with Convex Relaxation

Deepak Pullaguram, *Member, IEEE,* Ramtin Madani, *Member, IEEE,* Tuncay Altun, *Student Member, IEEE,* and Ali Davoudi, *Senior Member, IEEE*

***Abstract*—This paper details and solves a stability-constrained optimal power flow (SCOPF) for inverter-based AC microgrids. To ensure sufficient stability margin during optimal generation, a small-signal stability constraint is embedded into the conventional OPF formulation. This condition is enforced using a Lyapunov stability equation. A reduced-order model of the microgrid is adopted to alleviate the computational burden involved in solving the resulting SCOPF. Even then, the resulting stability conditions are highly non-linear and cannot be handled using the existing methods. To tackle the non-convexity in SCOPF due to the presence of the non-linear stability constraint, two distinct convex relaxation approaches, namely semi-definite programming and parabolic relaxations, are developed. A penalty function is added to the objective function of the relaxed SCOPF, which is, then, solved sequentially to obtain a feasible point. While off-the-shelf tools fail to produce any feasible point within hours, the proposed approach enables us to solve SCOPF in real-time. The efficacy of the proposed SCOPF is evaluated by performing numerical studies on multiple benchmarks as well as real-time studies on a 4-bus microgrid system built in a hardware-in-the-loop setup.**

***Index Terms*—AC Microgrids, Convex optimization, Optimal power flow, Relaxation, Stability.**

I. Introduction

MAJORITY of distributed generation units are interfaced with AC microgrids using inverters. Droop mechanism is a well-established decentralized control tool for proportional power sharing among inverters. This control approach alone does not ensure optimal operation or respect operational requirements usually dictated by the optimal power flows (OPFs) paradigms. An OPF-based droop adjustment is given in [1]. Varying droop parameters could cause small-signal stability issues [2], [3]. This paper provides an OPF paradigm that respects the small-signal stability margin, generation limits, power flow limits, and voltage constraints.

To enhance the stability margin, supplementary control loops [4], auxiliary stabilizers [5], [6], L_1-adaptive droop control [7], virtual droop frameworks [8], and lead compensators [9], are offered. These control methods are tuned for a selected range of operating points. Alternatively, an stability margin can be enforced by a proper generation dispatch via a holistic stability-constrained optimal power flow (SCOPF) formulation. SCOPF problem has already been studied in the context of conventional power systems [10]–[15].

D. Pullaguram was with the University of Texas at Arlington, USA. He is now with the National Institute of Technology, Warangal, India. R. Madani, T. Altun, and A. Davioudi are with the University of Texas at Arlington, USA. This research is funded, in part, by the Office of Naval Research under award N00014-18-1-2186, and approved for public release under DCN #43-6700-20.

SCOPF, with stability constraint dependent on state matrix sensitivities with respect to OPF variables, is detailed in [10], [11]. The stability constraint is presented as a semi-definite programming (SDP) problem in [12], and the resulting SCOPF is transformed to a non-linear optimization problem. SCOPF might lead to infeasible solutions due to its non-convex nature and the rigid threshold of the stability constraint [12]–[14]. To obtain a feasible solution, sequential quadratic programming and sequential optimization techniques, based on eigenvalue sensitivity matrix, are presented in [13] and [14], respectively. All these dispatching schemes are developed for conventional power systems with synchronous generators, and rely on interior-point methods that are sensitive to initial conditions. Alternatively, bilinear matrix inequalities (BMIs) can be employed to obtain optimal operating points ensuring stability margins. In [15], SCOPF problem is formulated for conventional power systems, where the stability constraint is developed using a BMI approach. The formulated SCOPF is convexified using SDP relaxation techniques, which could become computationally inefficient as the number of generators increases. The primary challenge tackled in this paper is the accommodation of highly non-linear matrix inequalities, resulted from enforcing stability conditions in inverter-based microgrids, that might not be within the reach of existing solvers. The key contributions can be summarized as follows:

- An illustrative example shows the susceptibility of OPF solutions for inverter-based AC microgrids to instability.
- SCOPF is formulated here by employing reduced-order dynamical model of inverter-based microgrids [16], and incorporating the Lyapunov stability equations that keeps system spectral abscissa below a certain threshold offering small-signal stability margin.
- While the existing optimization tools, e.g., PENBMI [17] and BMILAB [18], could not provide timely solutions for SCOPF, we solve the resulting non-linear and non-convex BMI equations using computationally-tractable SDP or parabolic relaxation techniques [19], [20].
- SCOPF is solved sequentially through objective penalization, to obtain feasible solutions that are beyond the reach of existing solvers.
- The penalized, relaxed SCOPF is experimentally validated for a 4-inverter microgrid system in a hardware-in-the-loop (HIL) environment under various loading scenarios.

II. Notations

The bold-italic upper case ($\boldsymbol{A}$), bold-italic lower case ($\boldsymbol{a}$), and italic lower case (a) indicate matrices, vectors, and scalars, respectively. $\mathbb{R}$ and $\mathbb{C}$ represent sets of real numbers, complex numbers, respectively. $\mathbb{S}^n$ and $\mathbb{H}^n$, respectively, indicate sets of $n \times n$ symmetric matrices and $n \times n$ hermitian matrices. The diagonal matrix with the '$\boldsymbol{a}$' vector of diagonal terms is shown by $[\boldsymbol{a}]$. $[\boldsymbol{a}]^n$ indicates the matrix formed by repeating the vector $\boldsymbol{a}$ for n columns. $(\cdot)^\top$ and $(\cdot)^*$ indicate the transpose and conjugate transpose of a matrix, respectively. $\mathbf{I}^n$ and 0^n indicate identity and zero matrices of size $n \times n$, respectively. The diagonal elements vector of a square matrix is shown by $\mathrm{diag}\{\cdot\}$. The vector or a scalar absolute value is given by $|\cdot|$. The trace of a matrix is shown by $\mathrm{tr}\{\cdot\}$. The frobenius norm of a matrix or a vector is represented by $\|\cdot\|$. The $\mathrm{Re}\{\cdot\}$ and $\mathrm{Im}\{\cdot\}$ indicates real and imaginary parts of the complex numbers, respectively. The notation $\boldsymbol{a}\cdot\boldsymbol{b}$ indicates the element-wise product of vectors $\boldsymbol{a}$ and $\boldsymbol{b}$.

The AC microgrid has $\mathcal{N} = \{1, 2, ..., n\}$ set of buses on the power distribution network, $\mathcal{L} = \{1, 2, ..., l\} \subseteq \mathcal{N} \times \mathcal{N}$ set of distribution lines, and $\mathcal{G} = \{1, 2, ..., n^{\mathrm{g}}\}$ set of inverters. The vectors of the injected active and reactive powers are $\boldsymbol{p}^{\mathrm{g}} \in \mathbb{R}^{n^{\mathrm{g}}\times 1}$ and $\boldsymbol{q}^{\mathrm{g}} \in \mathbb{R}^{n^{\mathrm{g}}\times 1}$, respectively. $\boldsymbol{d} \in \mathbb{C}^{n^{\mathrm{d}}\times 1}$ is the vector of power demand. An inverter and load incidence matrix, that locates inverters and loads on the distribution bus, is defined as $\boldsymbol{G} \in \{0,1\}^{n^{\mathrm{g}}\times n}$ and $\hat{\boldsymbol{D}} \in \{0,1\}^{n^{\mathrm{d}}\times n}$. The bus admittance matrix is given by $\boldsymbol{Y} \in \mathbb{C}^{n\times n}$. The $from$ and to admittance matrices are represented as $\vec{\boldsymbol{Y}}$, $\overleftarrow{\boldsymbol{Y}} \in \mathbb{C}^{n\times n}$, and their respective branch-incidence matrices as $\vec{\boldsymbol{L}}$, $\overleftarrow{\boldsymbol{L}} \in \{0,1\}^{l\times n}$. Loads are considered as constant complex impedances, and included as shunt elements in $\boldsymbol{Y}$. $\boldsymbol{v}^{\mathrm{g}} \in \mathbb{C}^{n^{\mathrm{g}}\times 1}$ is the vector of bus voltages at point of coupling, and $\boldsymbol{v}^{\mathrm{b}} \in \mathbb{C}^{n-n^{\mathrm{g}}\times 1}$ is the vector of all remaining buses, such that $\boldsymbol{v} = \boldsymbol{v}^{\mathrm{g}} \bigcup \boldsymbol{v}^{\mathrm{b}}$. $\boldsymbol{v}^{\mathrm{o}}$ is the terminal voltages at inverter output terminals.

III. Stability-constrained Optimal Power Flow

A. OPF in AC Microgrids

The OPF for an AC microgrid is formulated as

$$\begin{aligned}
\text{minimize} \quad & \mathrm{h}(\boldsymbol{p}^{\mathrm{g}}) && \text{(1a)}\\
\text{subject to} \quad & \boldsymbol{G}^\top(\boldsymbol{p}^{\mathrm{g}} + \mathrm{j}\boldsymbol{q}^{\mathrm{g}}) = \hat{\boldsymbol{D}}^\top \boldsymbol{d} + \mathrm{diag}\{\boldsymbol{v}\boldsymbol{v}^*\boldsymbol{Y}^*\} && \text{(1b)}\\
& \mathrm{diag}\{\vec{\boldsymbol{L}}\,\boldsymbol{v}\boldsymbol{v}^*\vec{\boldsymbol{Y}}^*\} \le \boldsymbol{f}^{\max} && \text{(1c)}\\
& \mathrm{diag}\{\overleftarrow{\boldsymbol{L}}\,\boldsymbol{v}\boldsymbol{v}^*\overleftarrow{\boldsymbol{Y}}^*\} \le \boldsymbol{f}^{\max} && \text{(1d)}\\
& \boldsymbol{p}^{\min} \le \boldsymbol{p}^g \le \boldsymbol{p}^{\max} && \text{(1e)}\\
& \boldsymbol{q}^{\min} \le \boldsymbol{q}^g \le \boldsymbol{q}^{\max} && \text{(1f)}\\
& (\boldsymbol{v}^{\min})^2 \le |\boldsymbol{v}|^2 \le (\boldsymbol{v}^{\max})^2 && \text{(1g)}\\
\text{varaibles} \quad & \boldsymbol{v} \in \mathbb{C}^{n\times 1}, \boldsymbol{p}^{\mathrm{g}} \in \mathbb{R}^{n^{\mathrm{g}}\times 1}, \boldsymbol{q}^{\mathrm{g}} \in \mathbb{R}^{n^{\mathrm{g}}\times 1}.
\end{aligned}$$

Here, $\mathrm{h}(\boldsymbol{p}^{\mathrm{g}})$ is assumed to be a quadratic cost function

$$\mathrm{h}(\boldsymbol{p}^{\mathrm{g}}) = (\boldsymbol{p}^{\mathrm{g}})^\top[\boldsymbol{c}_2]\tilde{\boldsymbol{p}}^{\mathrm{g}} + \boldsymbol{c}_1^\top\boldsymbol{p}^{\mathrm{g}} + \boldsymbol{c}_0^\top\mathbf{1}^{n_{\mathrm{g}}}, \tag{2}$$

where c_2, c_1, and c_0 are the cost coefficients. Quadratic cost functions are widely used in OPF problems even for inverter-based systems [21], [22]. The problem formulation, however, can be solved for any convex formulation of the cost function.

The nodal power balance is enforced using (1b). The line flows are limited in either directions using (1c) and (1d). The active and reactive powers generated by individual inverters are bounded using (1e) and (1f), respectively. The constraint (1g) bounds the voltage magnitude within $[\boldsymbol{v}^{\min}, \boldsymbol{v}^{\max}]$.

B. The Case for Stability-constrained OPF

The OPF alone cannot guarantee a stable operation for a microgrid. Consider an illustrative example of a three-bus, two-inverter microgrid shown in Fig 2. Primary droop control tunes individual inverters [23], in which the voltage reference ($\boldsymbol{v}^{\mathrm{ref}}$) and frequency reference ($\boldsymbol{\omega}^{\mathrm{ref}}$) are obtained using

$$\boldsymbol{\omega}^{\mathrm{ref}} = \omega_{\mathrm{nom}} - \boldsymbol{m}^p \cdot \boldsymbol{p} + \boldsymbol{m}^p \cdot \boldsymbol{p}^{\mathrm{opt}}, \tag{3}$$

$$\boldsymbol{v}^{\mathrm{ref}} = \boldsymbol{v}^{\mathrm{opt}} + \boldsymbol{n}^q \cdot \boldsymbol{q}^{\mathrm{opt}} - \boldsymbol{n}^q \cdot \boldsymbol{q}. \tag{4}$$

$\boldsymbol{p}$, $\boldsymbol{q}$ are the vectors of filtered active and reactive power of inverter, respectively. $\boldsymbol{p}^{\mathrm{opt}}$, $\boldsymbol{q}^{\mathrm{opt}}$, and $\boldsymbol{v}^{\mathrm{opt}}$ are the vector of active power, reactive power, and voltages set-points provided by the OPF. $\boldsymbol{m}_p$ and $\boldsymbol{n}_q$ are the vectors of $p-\omega$ and $q-v$ droop relations, respectively. Droop constants, used in the local primary control of inverters, are chosen as $m_p = 6.5 \times 10^{-4}$ (for the active power-frequency droop) and $n_q = 1.3 \times 10^{-3}$ (for the reactive power-voltage droop). Respective cost functions of inverters are formulated as $\mathrm{h}(p_1^{\mathrm{g}}) = 0.1(p_1^{\mathrm{g}})^2 + 20p_1^{\mathrm{g}}$ and $\mathrm{h}(p_2^{\mathrm{g}}) = 0.35(p_2^{\mathrm{g}})^2 + 20p_2^{\mathrm{g}}$. The microgrid operation, under conventional OPF, is shown in Fig. 3. When the power demand at bus 3 changes at $t = 2s$, the microgrid becomes unstable. This example illustrates the need to incorporate stability constraints in the OPF formulation. Next, additional constraints concerning system stability, inspired by the microgrid dynamics in [2], are needed to strengthen (1).

C. Incorporating Stability Constraint

To formulate the stability constraint, first, the microgrid is modeled as a set of differential-algebraic equations,

$$\dot{\boldsymbol{x}} = \boldsymbol{f}(\boldsymbol{x}, \boldsymbol{z}), \tag{5a}$$

$$0 = \boldsymbol{g}(\boldsymbol{x}, \boldsymbol{z}), \tag{5b}$$

where $\boldsymbol{f}$ and $\boldsymbol{g}$ represent the vectors of non-linear differential and algebraic equations of a microgrid, respectively. $\boldsymbol{x}$ and $\boldsymbol{z}$ are the vectors of state and algebraic variables of size n_{x} and n_{z}, respectively. To reduce the computational burden, a 3^{rd}-order inverter model [16] is adopted. The voltage and current controllers with LC filter in Fig. 1 have high closed-loop bandwidth compared to the power controller module, and one can safely assume that these control loops reach a quasi steady-state fast. Thus, the vector of differential equations, $\boldsymbol{f}$, with state variables $\boldsymbol{x} = [\boldsymbol{p}^\top, \boldsymbol{q}^\top, \boldsymbol{\delta}^\top]^\top \in \mathbb{R}^{n_{\mathrm{x}}\times 1}$, is composed of

$$\dot{\boldsymbol{p}} = -\boldsymbol{\omega}^c \cdot \boldsymbol{p} + \boldsymbol{\omega}^c \cdot \mathrm{Re}\{\boldsymbol{v}^{\mathrm{o}} \cdot (\boldsymbol{i}^{\mathrm{o}})^*\}, \tag{6a}$$

$$\dot{\boldsymbol{q}} = -\boldsymbol{\omega}^c \cdot \boldsymbol{q} + \boldsymbol{\omega}^c \cdot \mathrm{Im}\{\boldsymbol{v}^{\mathrm{o}} \cdot (\boldsymbol{i}^{\mathrm{o}})^*\}, \tag{6b}$$

$$\dot{\boldsymbol{\delta}} = (\boldsymbol{\omega} - \omega_{\mathrm{com}})\omega_{\mathrm{nom}}. \tag{6c}$$

Here, $\boldsymbol{\omega}_c \in \mathbb{R}^{n^{\mathrm{g}}\times 1}$ is the cutoff frequency of the low-pass filters used in power controller modules (Fig. 1). $\boldsymbol{p} \in \mathbb{R}^{n^{\mathrm{g}}\times 1}$

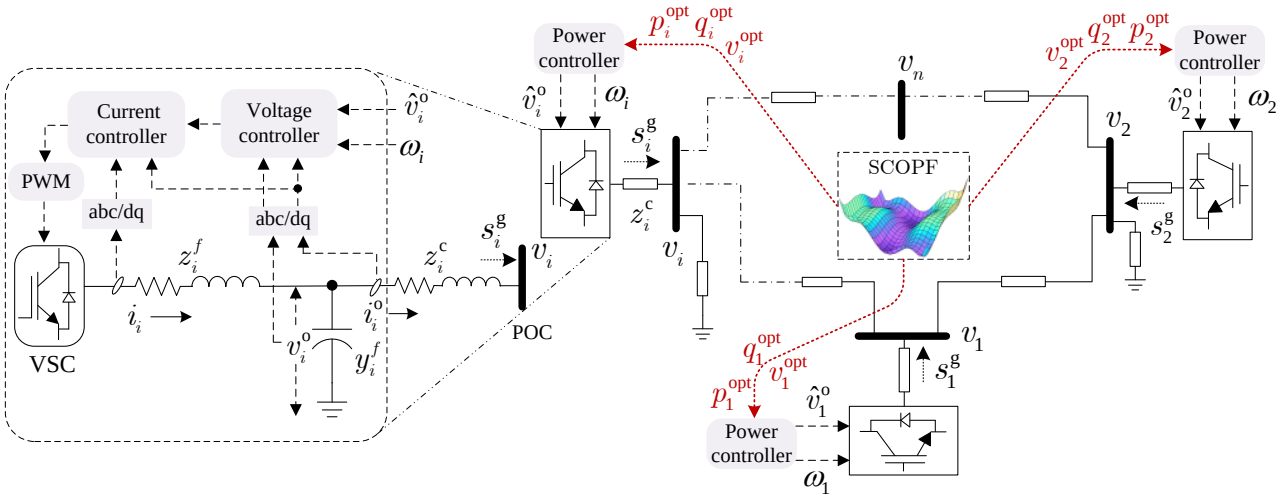

Fig. 1: AC microgrid schematic, inverter control, SCOPF optimization, and data flow.

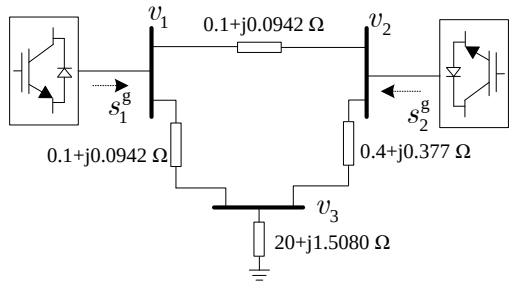

Fig. 2: A three-bus, two-inverter AC microgrid example system with line and load parameters.

and $\boldsymbol{q} \in \mathbb{R}^{n^{\mathrm{g}}\times 1}$ are the vectors of filtered active and reactive power, respectively. ω_{nom} and $\boldsymbol{\omega}$ are the microgrid nominal frequency and inverter operating frequency, respectively. $\boldsymbol{v}^{\mathrm{o}} \in \mathbb{C}^{n^{\mathrm{g}}\times 1} = \boldsymbol{v}^{\mathrm{od}} + \mathrm{j}\boldsymbol{v}^{\mathrm{oq}}$ and $\boldsymbol{i}^{\mathrm{o}} \in \mathbb{C}^{n^{\mathrm{g}}\times 1} = \boldsymbol{i}^{\mathrm{od}} + \mathrm{j}\boldsymbol{i}^{\mathrm{oq}}$ are the inverter terminal's voltage and current, respectively. $\boldsymbol{\delta}$ is the vector of inverter power angles with respect to a common reference, usually the inverter at bus 1 (i.e., $\omega_{\mathrm{com}} = \omega_1$). The operating frequency $\boldsymbol{\omega}$ is obtained using

$$\boldsymbol{\omega} \ = \omega_{\mathrm{nom}} - \boldsymbol{m}^{p} \cdot \boldsymbol{p} + \boldsymbol{m}^{p} \cdot \boldsymbol{p}^{\mathrm{opt}}, \tag{7}$$

where $\boldsymbol{p}^{\mathrm{opt}}$ is the active power set-point provided by the OPF, and $\boldsymbol{m}_p$ is the $p-\omega$ droop constant.

The vector of algebraic equations $\boldsymbol{g}$, with algebraic variables $\boldsymbol{z} = [(\boldsymbol{i}^{\mathrm{od}})^{\top}, (\boldsymbol{i}^{\mathrm{oq}})^{\top}]^{\top} \in \mathbb{R}^{n}_{\mathrm{z}} \times 1$, are given by

$$\boldsymbol{i}^{\mathrm{od}} = \mathrm{Re}\{\check{\boldsymbol{Y}}(\boldsymbol{v}^{\mathrm{o}} - \boldsymbol{i}^{\mathrm{o}} \cdot \boldsymbol{z}^{\mathrm{c}})\}, \tag{8a}$$

$$\boldsymbol{i}^{\mathrm{oq}} = \mathrm{Im}\{\check{\boldsymbol{Y}}(\boldsymbol{v}^{\mathrm{o}} - \boldsymbol{i}^{\mathrm{o}} \cdot \boldsymbol{z}^{\mathrm{c}})\}. \tag{8b}$$

$\check{\boldsymbol{Y}}$ is the Kron-reduced admittance matrix of the distribution network [16], $\boldsymbol{z}^{\mathrm{c}}$ is the impedance of the line connecting an inverter to the power distribution network, and

$$\boldsymbol{v}^{\mathrm{o}} = (\boldsymbol{v}^{\mathrm{opt}} + \boldsymbol{n}^{q} \cdot \boldsymbol{q}^{\mathrm{opt}} - \boldsymbol{n}^{q} \cdot \boldsymbol{q}) \cdot (\cos\boldsymbol{\delta} + \mathrm{j}\sin\boldsymbol{\delta}), \tag{9}$$

where $\boldsymbol{q}^{\mathrm{opt}}$ and $\boldsymbol{v}^{\mathrm{opt}}$ are the optimal reactive power and voltage set-points provided by the OPF, respectively. $\boldsymbol{n}_q$ is $q-v$ droop constant.

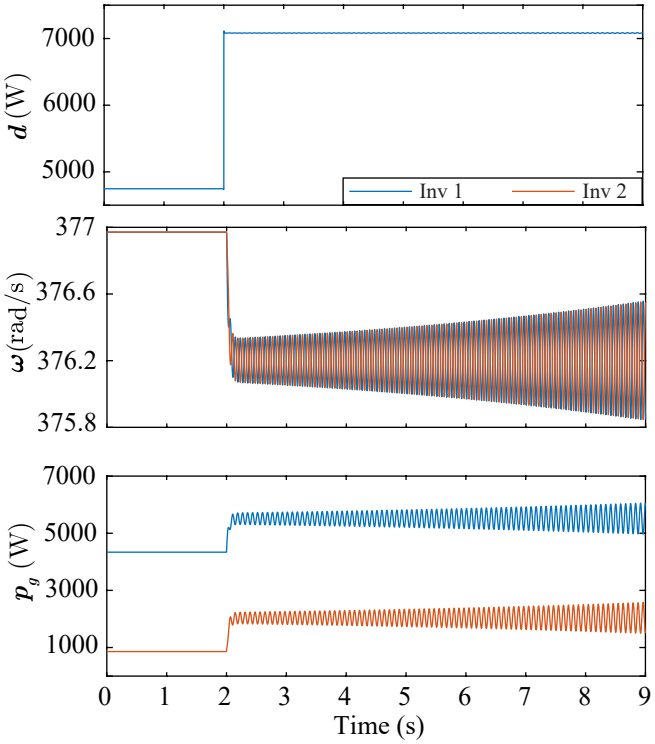

Fig. 3: Unstable microgrid operation with conventional OPF but without enforcing any stability constraint.

Proposition 1. *Consider a microgrid system defined by (5a) and (5b). Its small-signal stability, with a minimum decay rate($\propto$ damping ratio) of η, can be assured [24] iff there exits a symmetric positive definite matrix $\boldsymbol{M}$ that satisfies*

$$\hat{\boldsymbol{A}}^{\top}\boldsymbol{M} + \boldsymbol{M}\hat{\boldsymbol{A}} \preceq -2\eta\boldsymbol{M}, \tag{10}$$

where $\hat{\boldsymbol{A}}$ is the microgrid state matrix.

Proof. Linearizing (5a) and (5b) at the operating point

$$\frac{\partial \mathbf{f}}{\partial \boldsymbol{x}} = \begin{bmatrix} -[\boldsymbol{\omega}^{\mathrm{c}}] & -\Big[\boldsymbol{\omega}^{\mathrm{c}} \cdot \boldsymbol{n}^{q} \cdot (\boldsymbol{i}^{\mathrm{oq}} \cdot \sin\boldsymbol{\delta} + \boldsymbol{i}^{\mathrm{od}} \cdot \cos\boldsymbol{\delta})\Big] & -\Big[\boldsymbol{\omega}^{\mathrm{c}} \cdot (\boldsymbol{v}^{\mathrm{ref}} - \boldsymbol{n}^{q} \cdot \boldsymbol{q}) \cdot (\boldsymbol{i}^{\mathrm{od}} \cdot \sin\boldsymbol{\delta} - \boldsymbol{i}^{\mathrm{oq}} \cdot \cos\boldsymbol{\delta})\Big] \\ 0^{n^{\mathrm{g}}} & \Big[\boldsymbol{\omega}^{\mathrm{c}} \cdot \boldsymbol{n}^{\mathrm{q}} \cdot (\boldsymbol{i}^{\mathrm{oq}} \cdot \cos\boldsymbol{\delta} - \boldsymbol{i}^{\mathrm{od}} \cdot \sin\boldsymbol{\delta}) - \boldsymbol{\omega}^{\mathrm{c}}\Big] & \Big[\boldsymbol{\omega}^{\mathrm{c}} \cdot (\boldsymbol{v}^{\mathrm{ref}} - \boldsymbol{n}^{\mathrm{q}} \cdot \boldsymbol{q}) \cdot (\boldsymbol{i}^{\mathrm{od}} \cdot \cos\boldsymbol{\delta} + \boldsymbol{i}^{\mathrm{oq}} \cdot \sin\boldsymbol{\delta})\Big] \\ \boldsymbol{M}^{\mathrm{p}} & 0^{n^{\mathrm{g}}-1} & 0^{n^{\mathrm{g}}-1} \end{bmatrix} \tag{11}$$

$$\frac{\partial \mathbf{f}}{\partial \boldsymbol{z}} = \begin{bmatrix} \big[\boldsymbol{\omega}^{\mathrm{c}} \cdot (\boldsymbol{v}^{\mathrm{ref}} - \boldsymbol{n}^{\mathrm{q}} \cdot \boldsymbol{q}) \cdot \cos\boldsymbol{\delta}\big] & \big[\boldsymbol{\omega}^{\mathrm{c}} \cdot (\boldsymbol{v}^{\mathrm{ref}} - \boldsymbol{n}^{\mathrm{q}} \cdot \boldsymbol{q}) \cdot \sin\boldsymbol{\delta}\big] \\ \big[\boldsymbol{\omega}^{\mathrm{c}} \cdot (\boldsymbol{v}^{\mathrm{ref}} - \boldsymbol{n}^{\mathrm{q}} \cdot \boldsymbol{q}) \cdot \sin\boldsymbol{\delta}\big] & -\big[\boldsymbol{\omega}^{\mathrm{c}} \cdot (\boldsymbol{v}^{\mathrm{ref}} - \boldsymbol{n}^{\mathrm{q}} \cdot \boldsymbol{q}) \cdot \cos\boldsymbol{\delta}\big] \\ 0^{n\mathrm{g}-1} & 0^{n\mathrm{g}-1} \end{bmatrix} \tag{12}$$

$$\frac{\partial \mathbf{g}}{\partial \boldsymbol{x}} = \begin{bmatrix} 0^{n_{\mathrm{g}}} & (\check{\boldsymbol{G}} \cdot [\boldsymbol{n}^{\mathrm{q}} \cdot \cos\boldsymbol{\delta}]^{n^{\mathrm{g}}} - \check{\boldsymbol{B}} \cdot [\boldsymbol{n}^{\mathrm{q}} \cdot \sin\boldsymbol{\delta}]^{n^{\mathrm{g}}}) & \check{\boldsymbol{G}} \cdot [(\boldsymbol{v}^{\mathrm{ref}} - \boldsymbol{n}^{\mathrm{q}} \cdot \boldsymbol{q}) \cdot \sin\boldsymbol{\delta}]^{n^{\mathrm{g}}} + \check{\boldsymbol{B}}[(\boldsymbol{v}^{\mathrm{ref}} - \boldsymbol{n}^{\mathrm{q}} \cdot \boldsymbol{q}) \cdot \cos\boldsymbol{\delta}]^{n^{\mathrm{g}}} \\ 0^{n_{\mathrm{g}}} & (\check{\boldsymbol{G}} \cdot [\boldsymbol{n}^{\mathrm{q}} \cdot \sin\boldsymbol{\delta}]^{n^{\mathrm{g}}} + \check{\boldsymbol{B}} \cdot [\boldsymbol{n}^{\mathrm{q}} \cdot \cos\boldsymbol{\delta}]^{n^{\mathrm{g}}}) & \check{\boldsymbol{B}} \cdot [(\boldsymbol{v}^{\mathrm{ref}} - \boldsymbol{n}^{\mathrm{q}} \cdot \boldsymbol{q}) \cdot \sin\boldsymbol{\delta}]^{n^{\mathrm{g}}} - \check{\boldsymbol{G}}[(\boldsymbol{v}^{\mathrm{ref}} - \boldsymbol{n}^{\mathrm{q}} \cdot \boldsymbol{q}) \cdot \cos\boldsymbol{\delta}]^{n^{\mathrm{g}}} \end{bmatrix} \tag{13}$$

$$\frac{\partial \mathbf{g}}{\partial \boldsymbol{z}} = \begin{bmatrix} I^{n^{\mathrm{g}}} + \check{\boldsymbol{G}} \cdot [\boldsymbol{r_c}]^{n^{\mathrm{g}}} - \check{\boldsymbol{B}} \cdot [\boldsymbol{x_c}]^{n^{\mathrm{g}}} & -\check{\boldsymbol{G}} \cdot [\boldsymbol{x_c}]^{n^{\mathrm{g}}} - \check{\boldsymbol{B}} \cdot [\boldsymbol{r_c}]^{n^{\mathrm{g}}} \\ \check{\boldsymbol{B}} \cdot [\boldsymbol{r_c}]^{n^{\mathrm{g}}} + \check{\boldsymbol{G}} \cdot [\boldsymbol{x_c}]^{n^{\mathrm{g}}} & I^{n^{\mathrm{g}}} + \check{\boldsymbol{G}} \cdot [\boldsymbol{r_c}]^{n^{\mathrm{g}}} - \check{\boldsymbol{B}} \cdot [\boldsymbol{x_c}]^{n^{\mathrm{g}}} \end{bmatrix} \tag{14}$$

$(\boldsymbol{x}_0, \boldsymbol{z}_0)$, using Taylor series expansion, gives

$$\begin{bmatrix} \Delta\dot{\boldsymbol{x}} \\ \\ 0 \end{bmatrix} = \begin{bmatrix} \frac{\partial \boldsymbol{f}}{\partial \boldsymbol{x}} & \frac{\partial \boldsymbol{f}}{\partial \boldsymbol{z}} \\ \\ \frac{\partial \boldsymbol{g}}{\partial \boldsymbol{x}} & \frac{\partial \boldsymbol{g}}{\partial \boldsymbol{z}} \end{bmatrix} \begin{bmatrix} \Delta\boldsymbol{x} \\ \\ \Delta\boldsymbol{z} \end{bmatrix}. \tag{15}$$

The partial differential matrices $\frac{\partial \boldsymbol{f}}{\partial \boldsymbol{x}}$, $\frac{\partial \boldsymbol{f}}{\partial \boldsymbol{z}}$, $\frac{\partial \boldsymbol{g}}{\partial \boldsymbol{x}}$, and $\frac{\partial \boldsymbol{g}}{\partial \boldsymbol{z}}$ in (15) are given by (11)-(14), respectively. The $\boldsymbol{M}^{\mathrm{p}}$ in (11) is

$$\boldsymbol{M}^{\mathrm{p}} = \begin{bmatrix} -m_1^{\mathrm{p}} & m_2^{\mathrm{p}} & 0 & \cdots & 0 \\ -m_1^{\mathrm{p}} & 0 & m_3^{\mathrm{p}} & \cdots & 0 \\ \vdots & \vdots & \vdots & \ddots & 0 \\ -m_1^{\mathrm{p}} & 0 & 0 & \cdots & m_{n^g}^{\mathrm{p}} \end{bmatrix}, \tag{16}$$

where m_i^{p} indicates droop constant of i^{th} inverter. $\check{\boldsymbol{G}}$ and $\check{\boldsymbol{B}}$ are, respectively, the real and imaginary components of the Kron-reduced admittance matrix $\check{\boldsymbol{Y}}$.
Defining $\boldsymbol{A}(\boldsymbol{i}^{\mathrm{od}}, \boldsymbol{i}^{\mathrm{oq}}, \boldsymbol{\delta}, \boldsymbol{q}) = \frac{\partial \boldsymbol{f}}{\partial \boldsymbol{x}}$, $\boldsymbol{B}(\boldsymbol{\delta}, \boldsymbol{q}) = \frac{\partial \boldsymbol{f}}{\partial \boldsymbol{z}}$, $\boldsymbol{C}(\boldsymbol{\delta}, \boldsymbol{q}) = \frac{\partial \boldsymbol{g}}{\partial \boldsymbol{x}}$, and $\boldsymbol{D} = \frac{\partial \boldsymbol{g}}{\partial \boldsymbol{z}}$, and eliminating the algebraic variables $\boldsymbol{z}$, (15) can be reformulated [25] as,

$$\dot{\boldsymbol{x}} = \hat{\mathbf{A}}\boldsymbol{x}, \tag{17}$$

where $\hat{\boldsymbol{A}} \in \mathbb{R}^{n_{\mathrm{x}} \times n_{\mathrm{x}}}$ is the state matrix obtained by

$$\hat{\boldsymbol{A}} = \boldsymbol{A}(\boldsymbol{i}^{\mathrm{od}}, \boldsymbol{i}^{\mathrm{oq}}, \boldsymbol{\delta}, \boldsymbol{q}) - \boldsymbol{B}(\boldsymbol{\delta}, \boldsymbol{q})(\boldsymbol{D})^{-1}\boldsymbol{C}(\boldsymbol{\delta}, \boldsymbol{q}). \tag{18}$$

Consider a Lyapunov energy function, $V = \boldsymbol{x}^\top \boldsymbol{M}\boldsymbol{x}$, where $\boldsymbol{M} \in \mathbb{S}^{n_{\mathrm{x}}}$ is a symmetric positive definite matrix. Differentiating V, one has

$$\begin{aligned} \dot{V} &= \dot{\boldsymbol{x}}^\top \boldsymbol{M}\boldsymbol{x} + \boldsymbol{x}^\top \boldsymbol{M}\dot{\boldsymbol{x}}, \\ &= (\hat{\boldsymbol{A}}\boldsymbol{x})^\top \boldsymbol{M}\boldsymbol{x} + \boldsymbol{x}^\top \boldsymbol{M}\hat{\boldsymbol{A}}\boldsymbol{x}, \\ &= \boldsymbol{x}^\top (\hat{\boldsymbol{A}}^\top \boldsymbol{M} + \boldsymbol{M}\hat{\boldsymbol{A}})\boldsymbol{x}. \end{aligned} \tag{19}$$

For the microgrid to have a minimum damping (or decay rate) η, the necessary condition on the Lyapunov function [24] is

$$\dot{V} < -2\eta E. \tag{20}$$

From (19) and (20)

$$\hat{\boldsymbol{A}}^\top \boldsymbol{M} + \boldsymbol{M}\hat{\boldsymbol{A}} \preceq -2\eta \boldsymbol{M}, \tag{21a}$$

$$\boldsymbol{M} \succeq \mathrm{I}^{n_{\mathrm{x}}}. \tag{21b}$$

Proof of Proposition 1 is completed. □

From Proposition 1, the microgrid stability can be maintained by choosing η to be a small positive constant. η should be properly chosen, as a large η could lead to an infeasible solution, and a small η might not provide sufficient damping. Herein, η is selected in the range of $[0.5,\ 5]$.

To interlink the inverter internal variables with the OPF variables, additional constraints are formulated as

$$\boldsymbol{v}^{\mathrm{g}} = (\boldsymbol{v}^{\mathrm{ref}} - \boldsymbol{n}^{q} \cdot \boldsymbol{q}) \cdot (\cos\boldsymbol{\delta} + \mathrm{j}\sin\boldsymbol{\delta}) - \boldsymbol{i}^{\mathrm{o}} \cdot \boldsymbol{z}^{c}, \tag{22}$$

$$\boldsymbol{i}^{\mathrm{o}} = \check{\boldsymbol{Y}}\boldsymbol{v}^{\mathrm{g}}, \tag{23}$$

$$\boldsymbol{p} + \mathrm{i}\boldsymbol{q} = \mathrm{diag}\{\boldsymbol{i}^{\mathrm{o}}(\boldsymbol{i}^{\mathrm{o}})^*[\boldsymbol{z}^{\mathrm{c}}]\} + \boldsymbol{p}^{g} + \mathrm{i}\boldsymbol{q}^{g}. \tag{24}$$

The OPF in (1), with additional constraints (21)-(24), constitute a SCOPF for an inverter-dominant microgrid. The constraints (1b)-(1g) are quadratic functions of the bus voltage $\boldsymbol{v}$. The state matrix $\hat{\boldsymbol{A}}$ in (21a), and the constraints (22) and (24), are non-linear functions of $\boldsymbol{i}^{\mathrm{o}}$, $\boldsymbol{q}$, and $\boldsymbol{\delta}$. These non-linearities make problem non-convex. In the next section, the SCOPF problem is lifted and relaxed to make it computationally tractable.

IV. Lifting, Relaxation, and Penalization

A. Lifted Formulation

The constraints (1b)-(1g) can be convexified by defining an auxiliary matrix $\boldsymbol{W} \in \mathbb{H}^n$ [26] as

$$\boldsymbol{W} \triangleq \boldsymbol{v}\boldsymbol{v}^*. \tag{25}$$

To convexify the constraints (22) and (24), and the state matrix $\hat{\boldsymbol{A}}$ in (21a), variables $\boldsymbol{\delta}^{\mathrm{c}} \in \mathbb{R}^{n_{\mathrm{g}} \times 1}$, $\boldsymbol{\delta}^{\mathrm{s}} \in \mathbb{R}^{n_{\mathrm{g}} \times 1}$, $\boldsymbol{\delta}^{\mathrm{qc}} \in \mathbb{R}^{n_{\mathrm{g}} \times 1}$, $\boldsymbol{\delta}^{\mathrm{qs}} \in \mathbb{R}^{n_{\mathrm{g}} \times 1}$, and a new vector, $\boldsymbol{u}_k \in \mathbb{R}^{n_u \times 1}\ \forall\ k \in \mathcal{G}$, are defined for each inverter as

$$\boldsymbol{\delta}^{\mathrm{c}} \triangleq \cos\boldsymbol{\delta}, \qquad \boldsymbol{\delta}^{\mathrm{s}} \triangleq \sin\boldsymbol{\delta}, \tag{26a}$$

$$\boldsymbol{\delta}^{\mathrm{qc}} \triangleq \boldsymbol{q} \cdot \cos\boldsymbol{\delta}, \quad \boldsymbol{\delta}^{\mathrm{qs}} \triangleq \boldsymbol{q} \cdot \sin\boldsymbol{\delta}, \tag{26b}$$

$$\boldsymbol{u}_k \triangleq [i_k^{\mathrm{od}}, i_k^{\mathrm{oq}}, \delta_k^{\mathrm{c}}, \delta_k^{\mathrm{s}}, q_k, \delta_k^{\mathrm{qc}}, \delta_k^{\mathrm{qs}}]^\top\ \forall k \in \mathcal{G}. \tag{26c}$$

Using (26c), an auxiliary matrix for each inverter, $\boldsymbol{X}_k \in \mathbb{S}^{n_u}\ \forall\ k \in \mathcal{G}$, is defined as

$$\boldsymbol{X}_k \triangleq \boldsymbol{u}_k \boldsymbol{u}_k^\top, \tag{26d}$$

that satisfies a set of constraints $\mathcal{U}$ given as

$$(\boldsymbol{e}_k^{\delta^{\rm s}})^\top \boldsymbol{X}_k \boldsymbol{e}_k^{q} - \delta_k^{\rm qs} = 0, \tag{27a}$$
$$(\boldsymbol{e}_k^{\delta^{\rm c}})^\top \boldsymbol{X}_k \boldsymbol{e}_k^{q} - \delta_k^{\rm qc} = 0, \tag{27b}$$
$$(\boldsymbol{e}_k^{\delta^{\rm c}})^\top \boldsymbol{X}_k \boldsymbol{e}_k^{\delta^{\rm qs}} - (\boldsymbol{e}_k^{\delta^{\rm s}})^\top \boldsymbol{X}_k \boldsymbol{e}_k^{\delta^{\rm qc}} = 0, \tag{27c}$$
$$(\boldsymbol{e}_k^{\delta^{\rm c}})^\top \boldsymbol{X}_k \boldsymbol{e}_k^{\delta^{\rm c}} + (\boldsymbol{e}_k^{\delta^{\rm s}})^\top \boldsymbol{X}_k \boldsymbol{e}_k^{\delta^{\rm s}} - 1 = 0, \tag{27d}$$
$$(\boldsymbol{e}_k^{\delta^{\rm c}})^\top \boldsymbol{X}_k \boldsymbol{e}_k^{\delta^{\rm qc}} + (\boldsymbol{e}_k^{\delta^{\rm s}})^\top \boldsymbol{X}_k \boldsymbol{e}^{\delta_k^{\rm qs}} - q_k = 0, \tag{27e}$$
$$(\boldsymbol{e}_k^{\delta^{\rm qc}})^\top \boldsymbol{X}_k \boldsymbol{e}_k^{\delta^{\rm qc}} + (\boldsymbol{e}_k^{\delta^{\rm qs}})^\top \boldsymbol{X}_k \boldsymbol{e}_k^{\delta^{\rm qs}} - (\boldsymbol{e}_k^{q})^\top \boldsymbol{X}_k \boldsymbol{e}_k^{q} = 0. \tag{27f}$$

$\boldsymbol{e}_k^{i^{\rm od}}$, $\boldsymbol{e}_k^{i^{\rm od}}$, $\boldsymbol{e}_k^{\delta^{\rm c}}$, $\boldsymbol{e}_k^{\delta^{\rm s}}$, $\boldsymbol{e}_k^{q}$, $\boldsymbol{e}_k^{\delta^{\rm qc}}$, and $\boldsymbol{e}_k^{\delta^{\rm qs}}$ are the standard basis for respective elements of the vector $\boldsymbol{u}_k$.

From (25)-(26d), the constraints (1b)-(1g), (22), (24) and sub-matrices $\boldsymbol{A}(\boldsymbol{i}^{\rm od}, \boldsymbol{i}^{\rm oq}, \boldsymbol{\delta}, \boldsymbol{q})$, $\boldsymbol{B}(\boldsymbol{\delta}, \boldsymbol{q})$, and $\boldsymbol{C}(\boldsymbol{\delta}, \boldsymbol{q})$ can be reformulated as the linear functions of $\boldsymbol{u}_k$, and $\boldsymbol{X}_k$ as in (29), (30), (31), and (32). The state matrix $\hat{\boldsymbol{A}}$ and the stability constraint (21a) are still non-linear due to the presence of $\boldsymbol{B}\,(\boldsymbol{D})^{-1}\,\boldsymbol{C}$, $\hat{\boldsymbol{A}}^\top \boldsymbol{M}$, and $\boldsymbol{M}\hat{\boldsymbol{A}}$ terms. To overcome this, two auxiliary matrices, $\boldsymbol{E}$ and $\boldsymbol{L}$, are defined

$$\begin{aligned}\boldsymbol{E} &= \begin{bmatrix} \boldsymbol{E}^{\rm bb} & \boldsymbol{E}^{\rm bc} \\ \boldsymbol{E}^{\rm cb} & \boldsymbol{E}^{\rm cc} \end{bmatrix} \\ &\triangleq \begin{bmatrix} \boldsymbol{B}(\boldsymbol{\delta}^{\rm c}, \boldsymbol{\delta}^{\rm s}, \boldsymbol{\delta}^{\rm qc}, \boldsymbol{\delta}^{\rm qs}) \\ \hat{\boldsymbol{C}}^\top(\boldsymbol{\delta}^{\rm c}, \boldsymbol{\delta}^{\rm s}, \boldsymbol{\delta}^{\rm qc}, \boldsymbol{\delta}^{\rm qs}) \end{bmatrix} \begin{bmatrix} \boldsymbol{B}(\boldsymbol{\delta}^{\rm c}, \boldsymbol{\delta}^{\rm s}, \boldsymbol{\delta}^{\rm qc}, \boldsymbol{\delta}^{\rm qs}) \\ \hat{\boldsymbol{C}}^\top(\boldsymbol{\delta}^{\rm c}, \boldsymbol{\delta}^{\rm s}, \boldsymbol{\delta}^{\rm qc}, \boldsymbol{\delta}^{\rm qs}) \end{bmatrix}^\top \end{aligned} \tag{28a}$$

$$\boldsymbol{L} = \begin{bmatrix} \boldsymbol{L}^{\rm mm} & \boldsymbol{L}^{\rm ma} \\ \boldsymbol{L}^{\rm am} & \boldsymbol{L}^{\rm aa} \end{bmatrix} \triangleq \begin{bmatrix} \boldsymbol{M} \\ \hat{\boldsymbol{A}}^\top \end{bmatrix} [\boldsymbol{M}, \hat{\boldsymbol{A}}], \tag{28b}$$

where $\hat{\boldsymbol{C}}(\boldsymbol{\delta}^{\rm c}, \boldsymbol{\delta}^{\rm s}, \boldsymbol{\delta}^{\rm qc}, \boldsymbol{\delta}^{\rm qs}) = (\boldsymbol{D})^{-1}\boldsymbol{C}(\boldsymbol{\delta}^{\rm c}, \boldsymbol{\delta}^{\rm s}, \boldsymbol{\delta}^{\rm qc}, \boldsymbol{\delta}^{\rm qs})$. $\boldsymbol{D}$ is a constant matrix for a given distribution network.

The lifted formulation of the SCOPF is given in (29), where (29b)-(29l) are linear and convex. The non-convexity present in the original SCOPF is encapsulated by the constraints (29o)-(29r).

B. Convex Relaxation

To ensure that (29) is computationally tractable, non-convex constraints (29o)- (29r) are relaxed. This paper details two distinct relaxation approaches, a SDP relaxation and a computationally-efficient parabolic relaxation.

1) SDP relaxation: The SDP relaxation of the non-convex constraints in the lifted SCOPF problem (29) is given as

$$\boldsymbol{W} - \boldsymbol{v}\boldsymbol{v}^* \succeq 0, \tag{33a}$$
$$\begin{bmatrix} \boldsymbol{E}^{\rm bb} & \boldsymbol{E}^{\rm bc} \\ \boldsymbol{E}^{\rm cb} & \boldsymbol{E}^{\rm cc} \end{bmatrix} - \begin{bmatrix} \boldsymbol{B}(\boldsymbol{\delta}^{\rm c}, \boldsymbol{\delta}^{\rm s}, \boldsymbol{\delta}^{\rm qc}, \boldsymbol{\delta}^{\rm qs}) \\ \hat{\boldsymbol{C}}^\top(\boldsymbol{\delta}^{\rm c}, \boldsymbol{\delta}^{\rm s}, \boldsymbol{\delta}^{\rm qc}, \boldsymbol{\delta}^{\rm qs}) \end{bmatrix} \begin{bmatrix} \boldsymbol{B}(\boldsymbol{\delta}^{\rm c}, \boldsymbol{\delta}^{\rm s}, \boldsymbol{\delta}^{\rm qc}, \boldsymbol{\delta}^{\rm qs}) \\ \hat{\boldsymbol{C}}^\top(\boldsymbol{\delta}^{\rm c}, \boldsymbol{\delta}^{\rm s}, \boldsymbol{\delta}^{\rm qc}, \boldsymbol{\delta}^{\rm qs}) \end{bmatrix}^\top \succeq 0, \tag{33b}$$
$$\begin{bmatrix} \boldsymbol{L}^{\rm mm} & \boldsymbol{L}^{\rm ma} \\ \boldsymbol{L}^{\rm am} & \boldsymbol{L}^{\rm aa} \end{bmatrix} - \begin{bmatrix} \boldsymbol{M} \\ \hat{\boldsymbol{A}}^\top \end{bmatrix} [\boldsymbol{M}, \hat{\boldsymbol{A}}] \succeq 0, \tag{33c}$$
$$\boldsymbol{X}_k - \boldsymbol{u}_k {\boldsymbol{u}_k}^\top \succeq 0 \quad \forall\, k \in \mathcal{G}. \tag{33d}$$

$$\text{minimize} \quad \mathrm{h}(\boldsymbol{p}^{\rm g}) \tag{29a}$$
subject to

OPF constraints:

$$\boldsymbol{G}^\top(\boldsymbol{p} + j\boldsymbol{q}) = \hat{\boldsymbol{D}}^\top \boldsymbol{d} + \mathrm{diag}\{\boldsymbol{W}\boldsymbol{Y}^*\} \tag{29b}$$
$$\mathrm{diag}\{\vec{\boldsymbol{L}}\, \boldsymbol{W} \vec{\boldsymbol{Y}}^*\} \leq \boldsymbol{f}^{\max} \tag{29c}$$
$$\mathrm{diag}\{\bar{\boldsymbol{L}}\, \boldsymbol{W} \bar{\boldsymbol{Y}}^*\} \leq \boldsymbol{f}^{\max} \tag{29d}$$
$$\boldsymbol{p}^{\min} \leq \boldsymbol{p} \leq \boldsymbol{p}^{\max} \tag{29e}$$
$$\boldsymbol{q}^{\min} \leq \boldsymbol{q} \leq \boldsymbol{q}^{\max} \tag{29f}$$
$$(\boldsymbol{v}^{\min})^2 \leq \mathrm{diag}(\boldsymbol{W}) \leq (\boldsymbol{v}^{\max})^2 \tag{29g}$$
$$\boldsymbol{i}^{\rm o} = \boldsymbol{G}^\top \boldsymbol{Y} \boldsymbol{v} \tag{29h}$$
$$\boldsymbol{G}^\top \boldsymbol{v} = \boldsymbol{v}^{\rm ref} \cdot (\boldsymbol{\delta}^{\rm c} + \mathrm{j}\boldsymbol{\delta}^{\rm s}) - \boldsymbol{n}^q \cdot (\boldsymbol{\delta}^{\rm qc} + \mathrm{j}\boldsymbol{\delta}^{\rm qs}) - \boldsymbol{i}^{\rm o} \cdot \boldsymbol{z}^{\rm c} \tag{29i}$$
$$\begin{aligned} p_k + \mathrm{j}q_k = ((\boldsymbol{e}_k^{i^{\rm od}})^\top \boldsymbol{X}_k \boldsymbol{e}_k^{i^{\rm od}} + (\boldsymbol{e}_k^{i^{\rm oq}})^\top \boldsymbol{X}_k \boldsymbol{e}_k^{i^{\rm oq}}) z_k^{\rm c} \\ + p_k^g + \mathrm{j}q_k^q \quad \forall\, k \in \mathcal{G} \end{aligned} \tag{29j}$$

Stability constraints:

$$\boldsymbol{L}^{\rm am} + \boldsymbol{L}^{\rm ma} \preceq -2\eta \boldsymbol{M} \tag{29k}$$
$$\boldsymbol{M} \succeq \mathbf{I}^{n_{\rm x}} \tag{29l}$$

Auxiliary variable constraints:

$$\hat{\boldsymbol{A}} = \boldsymbol{A}(\boldsymbol{X}_k) - \boldsymbol{E} \quad \forall\, k \in \mathcal{G} \tag{29m}$$
$$\boldsymbol{u}_k = [i_k^{\rm od}, i_k^{\rm oq}, \delta_k^{\rm c}, \delta_k^{\rm s}, q_k, \delta_k^{\rm qc}, \delta_k^{\rm qs}]^\top \ \forall k \in \mathcal{G} \tag{29n}$$
$$\boldsymbol{W} = \boldsymbol{v}\boldsymbol{v}^* \tag{29o}$$
$$\begin{bmatrix} \boldsymbol{E}^{\rm bb} & \boldsymbol{E}^{\rm bc} \\ \boldsymbol{E}^{\rm cb} & \boldsymbol{E}^{\rm cc} \end{bmatrix} = \begin{bmatrix} \boldsymbol{B}(\boldsymbol{\delta}^{\rm c}, \boldsymbol{\delta}^{\rm s}, \boldsymbol{\delta}^{\rm qc}, \boldsymbol{\delta}^{\rm qs}) \\ \hat{\boldsymbol{C}}^\top(\boldsymbol{\delta}^{\rm c}, \boldsymbol{\delta}^{\rm s}, \boldsymbol{\delta}^{\rm qc}, \boldsymbol{\delta}^{\rm qs}) \end{bmatrix} \begin{bmatrix} \boldsymbol{B}(\boldsymbol{\delta}^{\rm c}, \boldsymbol{\delta}^{\rm s}, \boldsymbol{\delta}^{\rm qc}, \boldsymbol{\delta}^{\rm qs}) \\ \hat{\boldsymbol{C}}^\top(\boldsymbol{\delta}^{\rm c}, \boldsymbol{\delta}^{\rm s}, \boldsymbol{\delta}^{\rm qc}, \boldsymbol{\delta}^{\rm qs}) \end{bmatrix}^\top \tag{29p}$$
$$\begin{bmatrix} \boldsymbol{L}^{\rm mm} & \boldsymbol{L}^{\rm ma} \\ \boldsymbol{L}^{\rm am} & \boldsymbol{L}^{\rm aa} \end{bmatrix} = \begin{bmatrix} \boldsymbol{M} \\ \hat{\boldsymbol{A}}^\top \end{bmatrix} [\boldsymbol{M}\ \hat{\boldsymbol{A}}] \tag{29q}$$
$$\boldsymbol{X}_k = [i_k^{\rm od}, i_k^{\rm oq}, \delta_k^{\rm c}, \delta_k^{\rm s}, q_k, \delta_k^{\rm qc}, \delta_k^{\rm qs}]^\top [i_k^{\rm od}, i_k^{\rm oq}, \delta_k^{\rm c}, \delta_k^{\rm s}, q_k, \delta_k^{\rm qc}, \delta_k^{\rm qs}] \quad \forall\, k \in \mathcal{G} \tag{29r}$$
$$\boldsymbol{X}_k, [i_k^{\rm od}, i_k^{\rm oq}, \delta_k^{\rm c}, \delta_k^{\rm s}, q_k, \delta_k^{\rm qc}, \delta_k^{\rm qs}]^\top \in \mathcal{U} \quad \forall\, k \in \mathcal{G} \tag{29s}$$

variables

$\boldsymbol{v} \in \mathbb{C}^{n\times 1}$, $\boldsymbol{p}^{\rm g} \in \mathbb{R}^{n^{\rm g}\times 1}$, $\boldsymbol{q}^{\rm g} \in \mathbb{R}^{n^{\rm g}\times 1}$, $\boldsymbol{i}^{\rm o} \in \mathbb{C}^{n^{\rm g}\times 1}$,
$\boldsymbol{q} \in \mathbb{R}^{n^{\rm g}\times 1}$, $\boldsymbol{\delta}^{\rm c} \in \mathbb{R}^{n^{\rm g}\times 1}$, $\boldsymbol{\delta}^{\rm s} \in \mathbb{R}^{n^{\rm g}\times 1}$, $\boldsymbol{\delta}^{\rm qc} \in \mathbb{R}^{n^{\rm g}\times 1}$,
$\boldsymbol{\delta}^{\rm qs} \in \mathbb{R}^{n^{\rm g}\times 1}$, $\boldsymbol{M} \in \mathbb{S}^{n^{\rm g}}$, $\boldsymbol{W} \in \mathbb{H}^{n}$, $\hat{\boldsymbol{A}} \in \mathbb{R}^{n_{\rm x}\times n_{\rm x}}$,
$\boldsymbol{E} = \begin{bmatrix} \boldsymbol{E}^{\rm bb} & \boldsymbol{E}^{\rm bc} \\ \boldsymbol{E}^{\rm cb} & \boldsymbol{E}^{\rm cc} \end{bmatrix} \in \mathbb{R}^{2n_{\rm x}\times 2n_{\rm x}}$, $\boldsymbol{L} = \begin{bmatrix} \boldsymbol{L}^{\rm mm} & \boldsymbol{L}^{\rm ma} \\ \boldsymbol{L}^{\rm am} & \boldsymbol{L}^{\rm aa} \end{bmatrix} \in \mathbb{R}^{2n_{\rm x}\times 2n_{\rm x}}$,
and $\boldsymbol{X}_k \in \mathbb{R}^{n_u \times n_u} \forall\, k \in \mathcal{G}$.

where

$\mathcal{U}$ is set of constraints defined as (27),
The matrices $\boldsymbol{A}(\boldsymbol{X}_k)$, $\boldsymbol{B}(\boldsymbol{\delta}^{\rm c}, \boldsymbol{\delta}^{\rm s}, \boldsymbol{\delta}^{\rm qc}, \boldsymbol{\delta}^{\rm qs})$, and
$\boldsymbol{C}(\boldsymbol{\delta}^{\rm c}, \boldsymbol{\delta}^{\rm s}, \boldsymbol{\delta}^{\rm qc}, \boldsymbol{\delta}^{\rm qs})$ are defined as (30), (31), and (32), respectively.

Remark 1. *The constraints (33a)-(33d) can be cast as*

$$\begin{bmatrix} \boldsymbol{W} & \boldsymbol{v} \\ \boldsymbol{v}^* & 1 \end{bmatrix} \succeq 0, \tag{34}$$
$$\begin{bmatrix} \boldsymbol{E}^{\rm bb} & \boldsymbol{E}^{\rm bc} & \boldsymbol{B}^\top(\boldsymbol{\delta}^{\rm c}, \boldsymbol{\delta}^{\rm s}, \boldsymbol{\delta}^{\rm qc}, \boldsymbol{\delta}^{\rm qs}) \\ \boldsymbol{E}^{\rm cb} & \boldsymbol{E}^{\rm cc} & \hat{\boldsymbol{C}}^\top(\boldsymbol{\delta}^{\rm c}, \boldsymbol{\delta}^{\rm s}, \boldsymbol{\delta}^{\rm qc}, \boldsymbol{\delta}^{\rm qs}) \\ \boldsymbol{B}^\top(\boldsymbol{\delta}^{\rm c}, \boldsymbol{\delta}^{\rm s}, \boldsymbol{\delta}^{\rm qc}, \boldsymbol{\delta}^{\rm qs}) & \hat{\boldsymbol{C}}(\boldsymbol{\delta}^{\rm c}, \boldsymbol{\delta}^{\rm s}, \boldsymbol{\delta}^{\rm qc}, \boldsymbol{\delta}^{\rm qs}) & \mathbf{I}^{n_z} \end{bmatrix} \succeq 0, \tag{35}$$
$$\begin{bmatrix} \boldsymbol{L}^{\rm mm} & \boldsymbol{L}^{\rm ma} & \boldsymbol{M} \\ \boldsymbol{L}^{\rm am} & \boldsymbol{L}^{\rm aa} & \hat{\boldsymbol{A}}^\top \\ \boldsymbol{M} & \hat{\boldsymbol{A}} & \mathbf{I}^{n_x} \end{bmatrix} \succeq 0, \tag{36}$$
$$\begin{bmatrix} \boldsymbol{X}_k & \boldsymbol{u}_k \\ \boldsymbol{u}_k^\top & 1 \end{bmatrix} \succeq 0, \qquad \forall k \in \mathcal{G}. \tag{37}$$

$$\boldsymbol{A} = \begin{bmatrix} -[\boldsymbol{\omega}^{\mathrm{c}}] & -\left[\left(\omega_k^{\mathrm{c}} n_k^{\mathrm{q}}((\boldsymbol{e}_k^{i^{\mathrm{oq}}})^\top \boldsymbol{X}_k \boldsymbol{e}_k^{\delta^{\mathrm{s}}} + (\boldsymbol{e}_k^{i^{\mathrm{od}}})^\top \boldsymbol{X}_k \boldsymbol{e}_k^{\delta^{\mathrm{c}}})\right)_{k\in\mathcal{G}}\right] & -\left[\left(\omega_k^{\mathrm{c}}(v_k^{\mathrm{ref}}((\boldsymbol{e}_k^{i^{\mathrm{oq}}})^\top \boldsymbol{X}_k \boldsymbol{e}_k^{\delta^{\mathrm{s}}} + (\boldsymbol{e}_k^{i^{\mathrm{od}}})^\top \boldsymbol{X}_k \boldsymbol{e}_k^{\delta^{\mathrm{c}}}))\right)_{k\in\mathcal{G}}\right] + \\ & & \left[\left(\omega_k^{\mathrm{c}} n_k^{\mathrm{q}}(((\boldsymbol{e}_k^{i^{\mathrm{oq}}})^\top \boldsymbol{X}_k \boldsymbol{e}_k^{\delta^{\mathrm{qs}}} + (\boldsymbol{e}_k^{i^{\mathrm{od}}})^\top \boldsymbol{X}_k \boldsymbol{e}_k^{\delta^{\mathrm{qc}}}))\right)_{k\in\mathcal{G}}\right] \\ 0^{n^{\mathrm{g}}} & \left[\left(\omega_k^{\mathrm{c}} n_k^{\mathrm{q}}((\boldsymbol{e}_k^{i^{\mathrm{oq}}})^\top \boldsymbol{X}_k \boldsymbol{e}_k^{\delta^{\mathrm{c}}} - (\boldsymbol{e}_k^{i^{\mathrm{od}}})^\top \boldsymbol{X}_k \boldsymbol{e}_k^{\delta^{\mathrm{s}}}) - \omega_k^{\mathrm{c}}\right)_{k\in\mathcal{G}}\right] & \left[\left(\omega_k^{\mathrm{c}}(v_k^{\mathrm{ref}}((\boldsymbol{e}_k^{i^{\mathrm{od}}})^\top \boldsymbol{X}_k \boldsymbol{e}_k^{\delta^{\mathrm{c}}} + (\boldsymbol{e}_k^{i^{\mathrm{oq}}})^\top \boldsymbol{X}_k \boldsymbol{e}_k^{\delta^{\mathrm{s}}}))\right)_{k\in\mathcal{G}}\right] - \\ & & \left[\left(\omega_k^{\mathrm{c}} n_k^{\mathrm{q}}(((\boldsymbol{e}_k^{i^{\mathrm{od}}})^\top \boldsymbol{X}_k \boldsymbol{e}_k^{\delta^{\mathrm{qc}}} + (\boldsymbol{e}_k^{i^{\mathrm{oq}}})^\top \boldsymbol{X}_k \boldsymbol{e}_k^{\delta^{\mathrm{qs}}}))\right)_{k\in\mathcal{G}}\right] \\ \boldsymbol{M}^{\mathrm{p}} & 0^{n^{\mathrm{g}}-1} & 0^{n^{\mathrm{g}}-1} \end{bmatrix} \tag{30}$$

$$\boldsymbol{B} = \begin{bmatrix} \left[\left(\omega_k^{\mathrm{c}}(v_k^{\mathrm{ref}}\delta_k^{\mathrm{c}} - n_k^{\mathrm{q}}\delta_k^{\mathrm{qc}})\right)_{k\in\mathcal{G}}\right] & \left[\left(\omega_k^{\mathrm{c}}(v_k^{\mathrm{ref}}\delta_k^{\mathrm{s}} - n_k^{\mathrm{q}}\delta_k^{\mathrm{qs}})\right)_{k\in\mathcal{G}}\right] \\ \left[\left(\omega_k^{\mathrm{c}}(v_k^{\mathrm{ref}}\delta_k^{\mathrm{s}} - n_k^{\mathrm{q}}\delta_k^{\mathrm{qs}})\right)_{k\in\mathcal{G}}\right] & -\left[\left(\omega_k^{\mathrm{c}}(v_k^{\mathrm{ref}}\delta_k^{\mathrm{c}}) - n_k^{\mathrm{q}}\delta_k^{\mathrm{qc}})\right)_{k\in\mathcal{G}}\right] \\ 0^{n\mathrm{g}-1} & 0^{n\mathrm{g}-1} \end{bmatrix} \tag{31}$$

$$\hat{\boldsymbol{C}} = \boldsymbol{D}^{-1}\begin{bmatrix} 0^{n_{\mathrm{g}}} & \check{\boldsymbol{G}}\cdot[(n_k^{\mathrm{q}}\delta_k^{\mathrm{c}})_{k\in\mathcal{G}}]^{n^{\mathrm{g}}} - \check{\boldsymbol{B}}\cdot[(n_k^{\mathrm{q}}\delta_k^{\mathrm{s}})_{k\in\mathcal{G}}]^{n^{\mathrm{g}}} & \check{\boldsymbol{G}}\cdot[(v_k^{\mathrm{ref}}\delta_k^{\mathrm{s}} - n_k^{\mathrm{q}}\delta_k^{\mathrm{qs}})_{k\in\mathcal{G}}]^{n^{\mathrm{g}}} + \check{\boldsymbol{B}}\cdot[(v^{\mathrm{ref}_k}\delta_k^{\mathrm{c}} - n_k^{\mathrm{q}}\delta_k^{\mathrm{qc}})_{k\in\mathcal{G}}]^{n^{\mathrm{g}}} \\ 0^{n_{\mathrm{g}}} & \check{\boldsymbol{G}}\cdot[(n_k^{\mathrm{q}}\delta_k^{\mathrm{s}})_{k\in\mathcal{G}}]^{n^{\mathrm{g}}} + \check{\boldsymbol{B}}\cdot[(n_k^{\mathrm{q}}\delta_k^{\mathrm{c}})_{k\in\mathcal{G}}]^{n^{\mathrm{g}}} & \check{\boldsymbol{B}}\cdot[(v_k^{\mathrm{ref}}\delta_k^{\mathrm{s}} - n_k^{\mathrm{q}}\delta_k^{\mathrm{qs}})_{k\in\mathcal{G}}]^{n^{\mathrm{g}}} - \check{\boldsymbol{G}}[(v^{\mathrm{ref}_k}\delta_k^{\mathrm{c}} - n_k^{\mathrm{q}}\delta_k^{\mathrm{qc}})_{k\in\mathcal{G}}]^{n^{\mathrm{g}}} \end{bmatrix} \tag{32}$$

The above remark transforms the quadratic matrix inequalities (33b)-(33d) to convex linear matrix inequalities making the SCOPF more tractable. Nevertheless, with the increase in number of inverters and system size, solving SCOPF in (29) may become computationally challenging.

2) Parabolic relaxation: This is an alternative relaxation technique with a reduced computational burden. The non-convex problem is transformed to a convex quadratic constraint quadratic programming problem. The parabolic relaxation [26] of the non-convex voltage constraint, (29o), is given by

$$|v_j + v_k|^2 \le W_{jj} + W_{kk} + (W_{kj} + W_{jk}) \ \forall (j,k) \in \mathcal{L} \ (38a)$$
$$|v_j - v_k|^2 \le W_{jj} + W_{kk} - (W_{kj} + W_{jk}) \ \forall (j,k) \in \mathcal{L} \ (38b)$$
$$|v_j + \mathrm{j}v_k|^2 \le W_{jj} + W_{kk} - \mathrm{j}(W_{kj} - W_{jk}) \ \forall (j,k) \in \mathcal{L} \ (38c)$$
$$|v_j - \mathrm{j}v_k|^2 \le W_{jj} + W_{kk} + \mathrm{j}(W_{kj} - W_{jk}) \ \forall (j,k) \in \mathcal{L} \ (38d)$$
$$|v_j|^2 \le W_{jj} \qquad \forall j \in \mathcal{N}. \ (38e)$$

The parabolic relaxation of (29p)-(29r) can be obtained using the following proposition.

Proposition 2. *Assume $\boldsymbol{R} \in \mathbb{R}^{r\times s}$, $\boldsymbol{S} \in \mathbb{R}^{s\times r}$, and $\boldsymbol{T} \in \mathbb{S}^{2r}$ are the matrices expressed by*

$$\boldsymbol{T} = \begin{bmatrix} \boldsymbol{T}^{\mathrm{rr}} & \boldsymbol{T}^{\mathrm{rs}} \\ \boldsymbol{T}^{\mathrm{sr}} & \boldsymbol{T}^{\mathrm{ss}} \end{bmatrix} = [\boldsymbol{R}^\top, \ \boldsymbol{S}]^\top [\boldsymbol{R}^\top, \ \boldsymbol{S}]. \tag{38f}$$

The parabolic relaxation [19] is formulated as

$$T_{jj}^{\mathrm{rr}} + T_{kk}^{\mathrm{ss}} + 2T_{jk}^{\mathrm{rs}} \ge \|\boldsymbol{r}_j + \boldsymbol{s}_k\|^2 \ \ \forall j,k \in \{1,2,..,r\}, \ (38g)$$
$$T_{jj}^{\mathrm{rr}} + T_{kk}^{\mathrm{ss}} - 2T_{jk}^{\mathrm{rs}} \ge \|\boldsymbol{r}_j - \boldsymbol{s}_k\|^2 \ \ \forall j,k \in \{1,2,..,r\}. \ (38h)$$

Here, $\boldsymbol{r}_j$ and $\boldsymbol{s}_k$ are the j^{th} and k^{th} column vectors of the matrices $\boldsymbol{R}$ and $\boldsymbol{S}^\top$, respectively.

Proposition 2 convexifies the non-linear matrix equality constraints given by (29p)-(29r) using the parabolic relaxation technique. This approach relaxes the non-convex SCOPF problem into a tractable SCOPF problem. While the relaxed SCOPF problem is computationally tractable, it may not guarantee a feasible solution for the original problem in (1). Therefore, a sequential penalization approach is adopted.

C. Sequential Penalization

The solution obtained from the lifted problem (29a)-(29m) with the relaxed SCOPF constraints (34)-(37) or (38a)-(38h) may not be always feasible with the original problem (1). To resolve this, a linear penalty function ρ is added to the objective function in (29a)

$$\text{minimize } \mathrm{h}(\boldsymbol{p}^{\mathrm{g}}) + \rho(\boldsymbol{W}, \boldsymbol{v}, \boldsymbol{E}, \boldsymbol{B}, \hat{\boldsymbol{C}}, \boldsymbol{L}, \boldsymbol{M}, \hat{\boldsymbol{A}}, \boldsymbol{X}, \boldsymbol{u}) \ (39a)$$
$$\text{subject to (29b)-(29m)}, \ (39b)$$
$$\text{(34)-(37) SDP-relaxed constraints}, \ (39c)$$
$$\text{or}$$
$$\text{(38a)-(38h) Parabolic-relaxed constraints}, \ (39d)$$

where

$$\rho(\boldsymbol{W}, \boldsymbol{v}, \boldsymbol{E}, \boldsymbol{B}, \hat{\boldsymbol{C}}, \boldsymbol{L}, \boldsymbol{M}, \hat{\boldsymbol{A}}, \boldsymbol{X}, \boldsymbol{u}) \tag{40}$$
$$\triangleq (\mathrm{tr}\{\boldsymbol{W}\boldsymbol{P}\} - \boldsymbol{v}_0^*\boldsymbol{P}\boldsymbol{v} - \boldsymbol{v}^*\boldsymbol{P}\boldsymbol{v}_0 + \boldsymbol{v}_0^*\boldsymbol{P}\boldsymbol{v}_0) + \mu_1(\mathrm{tr}\{\boldsymbol{E}\} - 2\mathrm{tr}\{\boldsymbol{B}_0\boldsymbol{B}^\top\} - 2\mathrm{tr}\{\hat{\boldsymbol{C}}_0\hat{\boldsymbol{C}}^\top\} + \mathrm{tr}\{\boldsymbol{B}_0\boldsymbol{B}_0^\top\} + \mathrm{tr}\{\hat{\boldsymbol{C}}_0\hat{\boldsymbol{C}}_0^\top\})$$
$$\mu_2(\mathrm{tr}\{\boldsymbol{L}\} - 2\mathrm{tr}\{\boldsymbol{M}_0\boldsymbol{M}^\top\} - 2\mathrm{tr}\{\hat{\boldsymbol{A}}_0\hat{\boldsymbol{A}}^\top\} + \mathrm{tr}\{\boldsymbol{M}_0\boldsymbol{M}_0^\top\} + \mathrm{tr}\{\hat{\boldsymbol{A}}_0\hat{\boldsymbol{A}}_0^\top\}) + \mu_3\mathrm{tr}\{\boldsymbol{X}_k - 2\boldsymbol{u}_{0_k}\boldsymbol{u}_k^\top + \boldsymbol{u}_{0_k}\boldsymbol{u}_{0_k}^\top\}. \tag{41}$$

$\boldsymbol{v}_0, \boldsymbol{B}_0, \hat{\boldsymbol{C}}_0, \boldsymbol{M}_0, \hat{\boldsymbol{A}}_0, \boldsymbol{u}_{0_k}$ are the given initial values. μ_1, μ_2, and μ_3 are the penalty positive coefficients valued at 0.1, 0.5, and 5, respectively. Here, $\boldsymbol{P}$ is the penalty function coefficient matrix for the voltage which can be calculated as in [26].

For an arbitrary initial point, the SCOPF (39) is solved sequentially until a feasible solution to (1) is obtained. It can then reduce the value of the objective function in subsequent iterations until a near optimal solution is found [19], [20]. The flow chart for solving sequential penalized SCOPF problem is shown in Fig.4. The penalized SCOPF is solved till the ε is less than considered threshold value. Here ε is given as,

$$\varepsilon = \max(||\boldsymbol{v} - \boldsymbol{v}_0||, ||\boldsymbol{B} - \boldsymbol{B}_0||, ||\hat{\boldsymbol{C}} - \hat{\boldsymbol{C}}_0||, ||\boldsymbol{M} - \boldsymbol{M}_0||, ||\hat{\boldsymbol{A}} - \hat{\boldsymbol{A}}_0||, ||\boldsymbol{u}_k - \boldsymbol{u}_{0_k}||). \tag{42}$$

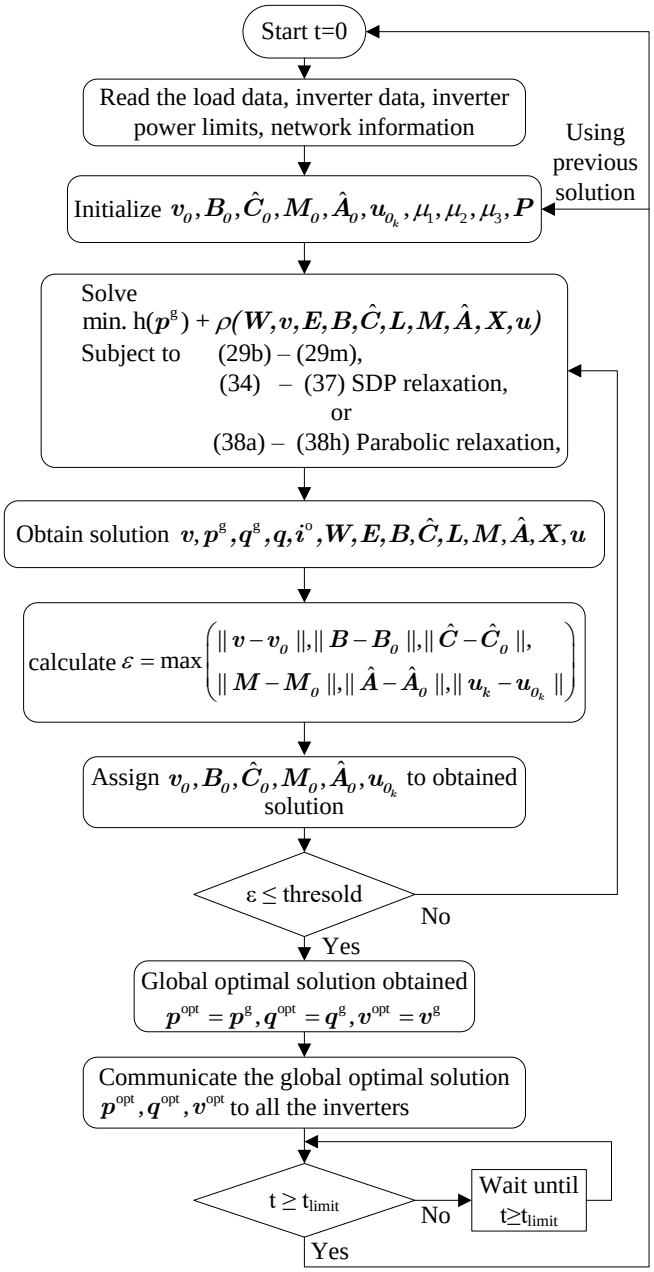

Fig. 4: Steps of the sequential penalized SCOPF solution.

V. Validation and Verification

A. Numerical Studies

The efficacy of both SDP and parabolic convex relaxations are evaluated on several standard test systems. All numerical studies are performed in MATLAB/CVX platform using MOSEK solver [27], on a 64-bit personal computer (PC) with 3.4GHz Intel i7 quadcore processor and 64 GB RAM. The droop constants $\boldsymbol{m}^{\mathrm{p}} = 1.5 \times 10^{-4}$ and $\boldsymbol{n}^{\mathrm{q}} = 7.2 \times 10^{-4}$, and the minimum decay rate of $\eta = 1$, are chosen.

In Table I, upper bound (UB) indicates the optimal cost obtained after sequential penalization, Lower bound (LB) indicates the optimal cost obtained for the relaxed problem without penalty, and computational time indicates the time taken by the optimization solver to solve the relaxed problem without sequential penalization. From Table I, for smaller systems with less number of inverters, the SDP relaxation offers LBs closer to the optimal solution with similar computational time as compared to parabolic relaxation. As the number of inverters and system size increases, SDP becomes computationally more expensive.

B. Hardware-in-the-Loop Validation

The proposed SCOPF is tested on a 4-bus, 4-inverter microgrid system [28], shown in Fig. 5. Inverters power limits and their cost coefficients are detailed in Table II. The microgrid's base power and voltage are $0.1MVA$ and $480V$, respectively. The nominal frequency of the microgrid is $\omega_{\mathrm{nom}} = 377rad/s$. This microgrid has variable-impedance loads, with 0.707 lagging power factor, at all buses. The complete microgrid is emulated in two Typhoon HIL604 units. Inverters employ droop control schemes with $\boldsymbol{m}^{\mathrm{p}} = 1.04 \times 10^{-4}$ (for the active power-frequency droop) and $\boldsymbol{n}^{\mathrm{q}} = 2.3 \times 10^{-4}$ (for the reactive power-voltage droop). These controllers are realized using two dSPACE MLBx control boxes with a 100μs sampling rate. A personal computer (PC) with an 8-core, 3.5GHz Xeon processor, and 64GB RAM solves the SCOPF using MATLAB/CVX

TABLE I: Upper bounds, lower bounds, and computational times for SCOPF with SDP and parabolic relaxations.

Test system	n^g	UB	SDP		Parabolic	
			LB	time (s)	LB	time (s)
9-bus	3	4234.76	3984.51	0.44	3900.42	0.42
14-bus	5	7963.32	7076.86	0.61	6561.84	0.53
30-bus	6	563.15	523.77	0.95	498.90	0.61
57-bus	7	43728.37	39803.98	2.88	35740.58	1.26
39-bus	10	39241.56	33307.43	6.83	32607.87	3.33
89pegase	12	5830.64	5127.92	19.95	4226.49	8.69
24_ieee_rts	33	-	56877.63	3487.61	53263.30	728.30

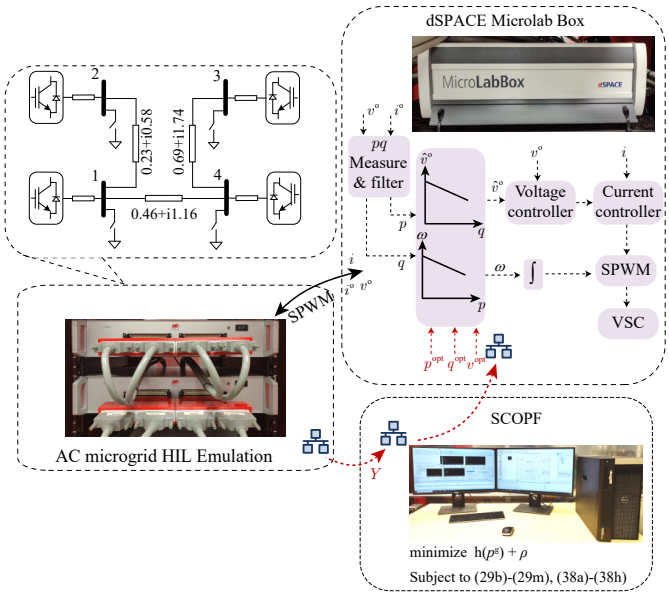

Fig. 5: The microgrid test system implemented using HIL (Typhoon HIL), control unit (dSPACE), and optimization unit (personal computer), with information flow shown.

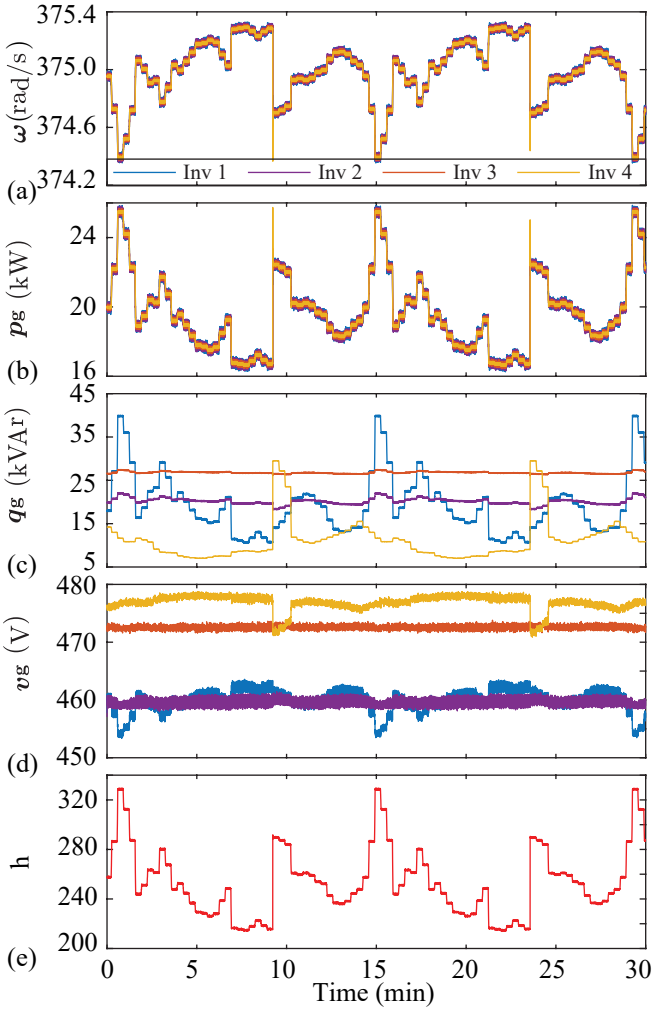

Fig. 6: Operation with droop control and varying loads at bus 1 and 4: (a) frequency, (b) active power generation, (c) reactive power generation, (d) voltage magnitude, and (e) total generation cost.

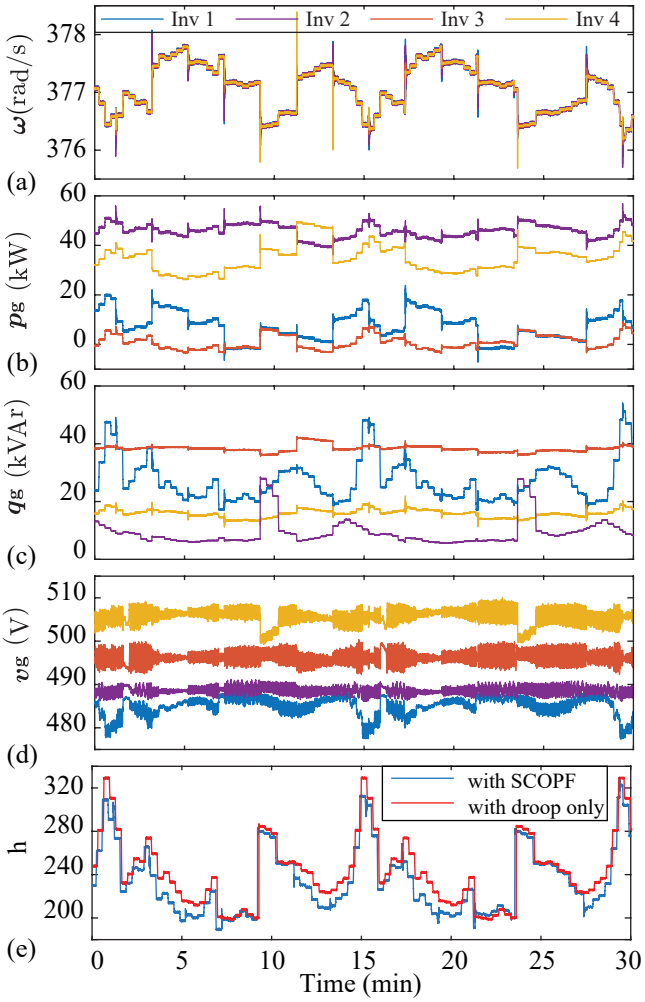

Fig. 7: Microgrid operation with SCOPF and varying loads at bus 1 and 4: (a) frequency, (b) active power generation, (c) reactive power generation, (d) voltage magnitude, and (e) total generation cost.

optimization tool with a MOSEK solver [27]. The stability constraint threshold in SCOPF is chosen as $\eta = 1$. The PC reads the microgrid information from the HIL emulator every two minutes, solves the penalized relaxed SCOPF problem, and sends the optimal solution to the control boxes. The information sharing between the HIL emulator and the PC, and the PC and control boxes, is carried out using Ethernet communication.

1) Microgrid performance without and with SCOPF: The microgrid system is emulated in the HIL environment for 30 minutes. Every 20 seconds, loads at all buses are randomly varied following a poisson distribution. Figures 6 and 7 depict the microgrid operation without and with SCOPF, respectively. Without SCOPF, the set-point values were held constant at $\boldsymbol{p}^{\text{opt}} = 0$, $\boldsymbol{q}^{\text{opt}} = 0$, and $\boldsymbol{v}^{\text{opt}} = 480V$. The voltages and the reactive power generations are within the limits for both scenarios, as shown in Fig. 6(c),(d) and Fig. 7(c),(d). The active power load variations are shared equally among all the inverters due to the constant active power set-point ($\boldsymbol{p}^{\text{opt}}$) and identical droop constants ($\boldsymbol{m}^{\text{p}}$), as shown in Fig.

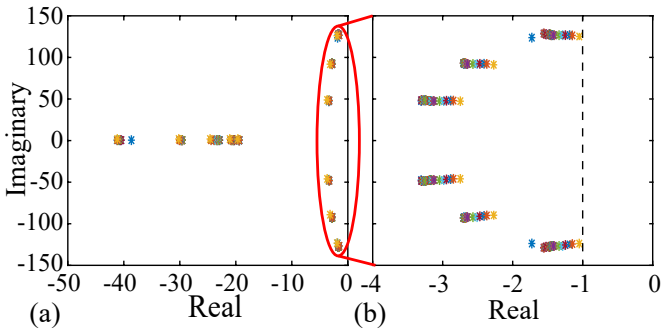

Fig. 8: (a) Microgrid eigenvalues with varying load conditions under SCOPF, (b) Zoomed-in view of the plot.

6(b). On the contrary, using SCOPF, the optimal set-points are provided at every 2 minutes, leading to unequal, but cost effective powers supplied by the inverters, as shown in Fig. 7(b). The average total generation cost for 30 minutes, with the droop control alone, is 253.5723. Using SCOPF, the average total generation cost reduces to 233.7836. Figure 8 shows the traces of eigenvalues at different optimal set-points provided by SCOPF under varying load conditions. It can be observed that the real part of eigenvalues are always kept less than -1, which is expected as $\eta = 1$. Moreover, it can be observed from Fig. 6(a) and 7(a) that the operating frequency, with the droop control alone, deviates further from the nominal value (ω_{nom}) compared to when SCOPF is employed.

TABLE II: Generational cost coefficients and power limits

Bus	c_2	c_1	c_0	$p^{\min}$	$p^{\max}$	$q^{\min}$	$q^{\max}$
1	1.3	2.2	0	0	1.0	-0.80	0.80
2	1.6	2.8	0	0	1.0	-0.80	0.80
3	2.0	5.5	0	0	1.0	-0.80	0.80
4	1.6	2.4	0	0	1.0	-0.80	0.80

2) Comparing conventional OPF and SCOPF: The advantage of SCOPF over the conventional OPF is demonstrated here. Figures 9 and 10 portray the microgrid performance with the operating set-points dictated by OPF and SCOPF, respectively. In both scenarios, initially, the microgrid operates with load impedance of $(5+i5)\ \Omega$ at all buses. At $t = t_1$, the load at bus 3 is disconnected. Set-points provided by SCOPF lead to better damping as compared to that of conventional OPF, as observed from Fig. 9(a) and Fig. 10(a). At $t = t_2$, the load is added back to bus 3. The microgrid driven by OPF exhibits negative damping leading to an oscillatory instability, while SCOPF provides stable operation with a positive damping. Microgrid eigenvalues, under OPF and SCOPF, are shown in Fig. 11(a) and Fig. 11(b), respectively. Under the conventional OPF, two eigenvalues are very close to the imaginary axis which, with a small perturbation in load, could shift to the right side of the imaginary axis and make the microgrid unstable. By contrast, under SCOPF, the eigenvalues are further away from the imaginary axis to provide a stability margin.

3) Microgrid performance with varying load and generation limits: The SCOPF operation, under correlated variation in generation limits and load demand based on weather conditions, is considered. The generation limits of all inverters, as well as the load demand at bus 1 and 4, are varied using a common Markov transition probability matrix ($\hat{\boldsymbol{M}}$) that provides probabilities of the transition of weather conditions based on the initial state vector $\hat{\boldsymbol{t}}$ as given in [29]. For simplicity, three possible weather conditions are considered as '*good*', '*normal*', and '*bad*'. For these conditions, $\hat{\boldsymbol{M}}$ is defined as

$$\hat{\boldsymbol{M}} = \begin{bmatrix} 0.96 & 0.02 & 0.02 \\ 0.02 & 0.96 & 0.02 \\ 0.02 & 0.02 & 0.96 \end{bmatrix}. \tag{43}$$

The distribution of initial state vector $\hat{\boldsymbol{t}}$ is considered as

$$\hat{\boldsymbol{t}} = \begin{bmatrix} 0.02 & 0.96 & 0.02 \end{bmatrix}^{\top}. \tag{44}$$

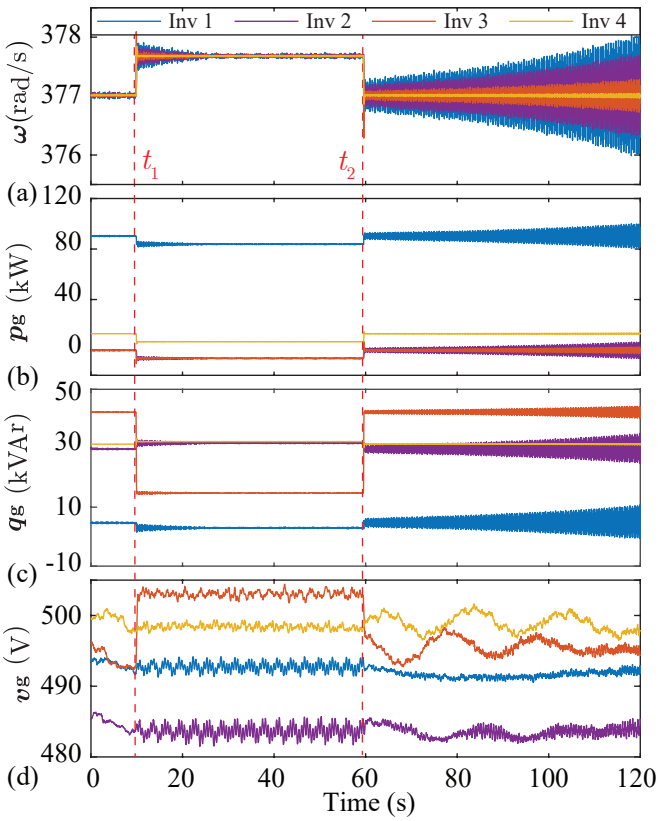

Fig. 9: Microgrid performance with optimal set-points provided by conventional OPF with the load at bus 3 disconnected and reconnected at $t = t_1$ and $t = t_2$: (a) frequency, (b) active power generation, (c) reactive power generation, and (d) voltage magnitude.

The correlated transition of generation limits and load demand are shown in Figs. 12(b) and 12(c), respectively. The generation limits and loads are varied based on the occurrence of these conditions. Based on the transition matrix, if the '*good*' weather occurs, the generation limits are increased by 10% and the loads are decreased by 15% from their rated values. If the '*bad*' weather happens, the generation limits are decreased by 15% and the loads are increased by 10% from their rated values. The active powers generated by all inverters are held within the varying generation limits, as observed from Figs. 12(b) and 12(d). Throughout, the limits on the reactive powers are varied keeping the MVA rating of any individual inverter constant at 0.1 MVA.

C. Incorporating Constant Power Loads in SCOPF

A detailed dynamic model of an inverter-based AC microgrid, with constant power loads, is adopted from [30]. Stability constraints of microgrid using this detailed dynamic model are

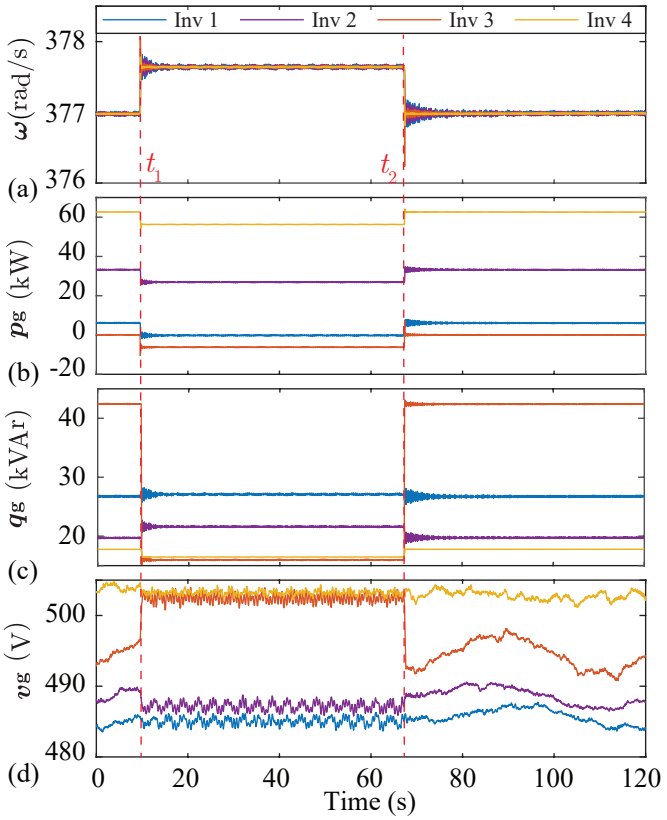

Fig. 10: Microgrid performance with optimal set-points provided by SCOPF with the load at bus 3 disconnected and reconnected at $t = t_1$ and $t = t_2$: (a) frequency, (b) active power generation, (c) reactive power generation, and (d) voltage magnitude.

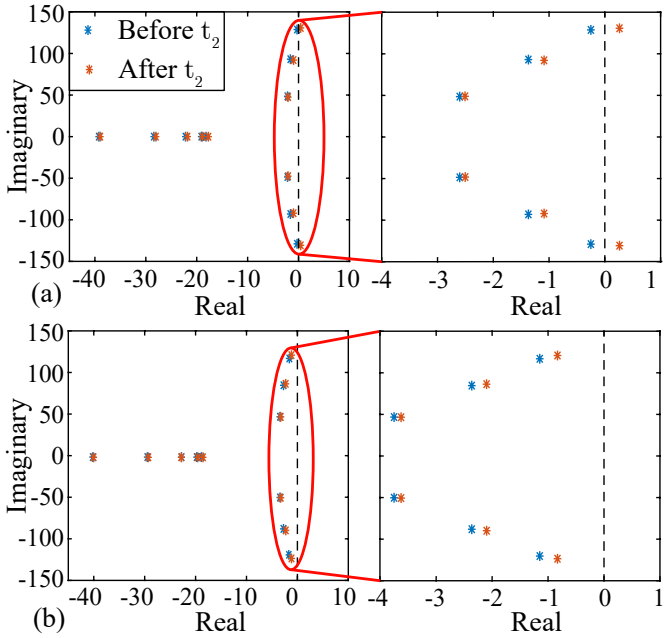

Fig. 11: Microgrid eigenvalues under (a) OPF, (b) SCOPF. * indicates eigenvalues before the load disturbance at $t = t_2$ and * indicates eigenvalues after $t = t_2$.

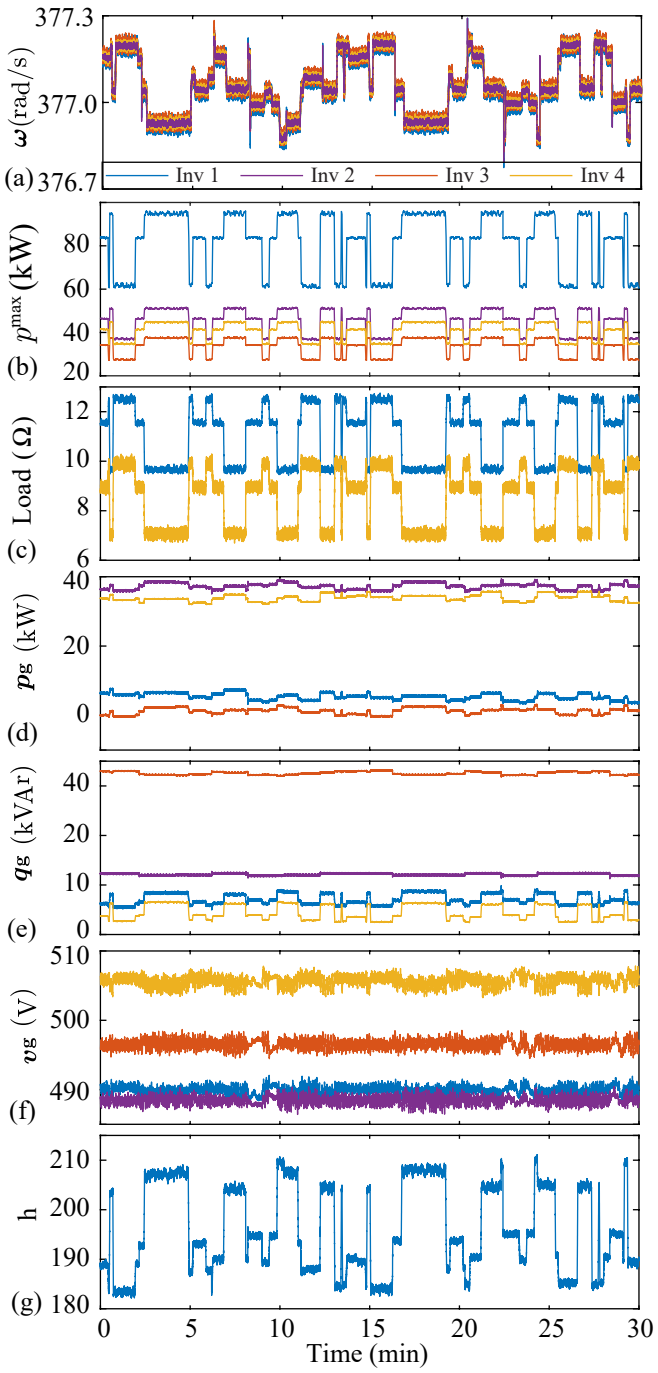

Fig. 12: Microgrid operation with SCOPF under the correlated variation of loads and generation limits: (a) frequency, (b) generation limits, (c) load at buses 1 and 4, (d) active power generation, (e) reactive power generation, (f) voltage magnitude, and (g) total generation cost.

modified as

$$\boldsymbol{A}^\top \boldsymbol{M} + \boldsymbol{M}\boldsymbol{A} \preceq -2\eta \boldsymbol{M}, \tag{45}$$

$$\boldsymbol{M} \succeq \mathrm{I}^{n_x}, \tag{46}$$

$$\boldsymbol{v}\vec{\boldsymbol{Y}} = \boldsymbol{i}^l, \tag{47}$$

$$\boldsymbol{i}^{\mathrm{d}} = \hat{\boldsymbol{D}}\boldsymbol{v} \cdot \frac{1}{\boldsymbol{z}^{\mathrm{d}}}, \tag{48}$$

where $\boldsymbol{z}^{\mathrm{d}}$ is the load impedance and $\hat{\boldsymbol{D}}$ is the load incidence matrix. $\boldsymbol{A}$ is a state matrix of the full-order dynamic model of the inverter-based AC microgrid [30]. The impedance of the constant power load, at bus j, is dynamically calculated using $z^{\mathrm{d}} = v_j^2/p_j^{\mathrm{d}} + \mathrm{j}\omega_0 L_j^{\mathrm{d}}$, and included in the state matrix $\boldsymbol{A}$ as given in [30]. p_j^{d} is the active power demand, and L_j^{d} is the series inductance associated with the constant power load.

Similar to the previously-presented case of constant impedance loads, SCOPF formulation with constant power loads would also includes non-linear terms. Similar lifting and relaxation techniques detailed in Section IV can be used to convexify the resulting SCOPF formulation. One should note the difference in system matrices for the reduced-order and full-order models. For the microgrid example considered here, the size of the state matrix of the full-order model including the constant power load, $\boldsymbol{A}$, is 65×65, whereas, the size of the state matrix using the reduced-order model with constant impedance load, $\hat{\boldsymbol{A}}$, is 11×11. To the best of our knowledge, a reduced-order model of AC microgrids, with constant power loads, is not yet available in the literature.

In the next study, SCOPF for a microgrid with constant power loads is illustrated. Constant power loads are connected at buses 1 and 4, as seen in Fig .13(b). Initially, inverters operate with local droop mechanisms that caused the drop in frequency (Fig. 13(a)) and voltage (Fig. 13(e)) from their nominal values of $377rad/s$ and $480V$, respectively. The overall load demand is shared proportionally among all inverters as shown in Fig. 13(c). At $t = t_1$, all inverters are provided with the stable optimal set-points obtained from SCOPF, and adjust their outputs accordingly, as shown in Fig.13(f).

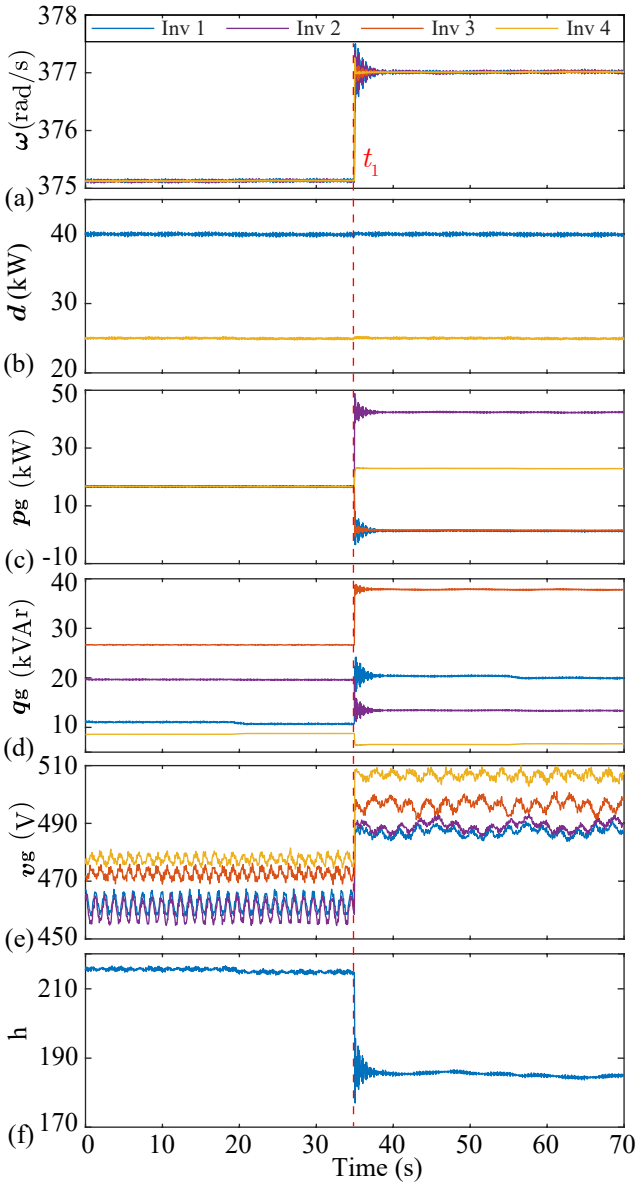

Fig. 13: SCOPF with constant power loads: (a) frequency, (b) constant power loads at buses 1 and 4, (c) active power generation, (d) reactive power generation, (e) voltage magnitude, and (f) total generation cost.

VI. Conclusion

This paper addresses the stable and optimal operation of inverter-populated AC microgrid. SCOPF provides the optimal operating set-points to the inverters and exhibits improved damping characteristics as compared to the operation provided by the conventional OPF. The stability constraints for the SCOPF is formulated as a bilinear matrix inequality (BMI) constraint derived from a Lyapunov stability candidate. The SCOPF formulation is non-convex due to the presence of multiple non-linear terms. To make it computationally efficient, we have relaxed this problem using two distinct convex relaxation techniques, namely, SDP and parabolic relaxations. To prove solution scalability, several numerical studies were carried out on multiple standard IEEE and European test systems. Further, the feasibility and the efficacy of the proposed SCOPF is evaluated on a 4-inverter microgrid system emulated in a HIL setup.

References

[1] G. Agundis-Tinajero, N. L. D. Aldana, A. C. Luna, J. Segundo-Ramírez, N. Visairo-Cruz, J. M. Guerrero, and J. C. Vazquez, "Extended-optimal-power-flow-based hierarchical control for islanded ac microgrids," *IEEE Transactions on Power Electronics*, vol. 34, pp. 840–848, Jan 2019.

[2] N. Pogaku, M. Prodanovic, and T. C. Green, "Modeling, analysis and testing of autonomous operation of an inverter-based microgrid," *IEEE Transactions on Power Electronics*, vol. 22, pp. 613–625, March 2007.

[3] R. Majumder, "Some aspects of stability in microgrids," *IEEE Transactions on Power Systems*, vol. 28, no. 3, pp. 3243–3252, Aug 2013.

[4] R. Majumder, B. Chaudhuri, A. Ghosh, R. Majumder, G. Ledwich, and F. Zare, "Improvement of stability and load sharing in an autonomous microgrid using supplementary droop control loop," *IEEE Transactions on Power Systems*, vol. 25, no. 2, pp. 796–808, May 2010.

[5] A. Kahrobaeian and Y. A. I. Mohamed, "Analysis and mitigation of low-frequency instabilities in autonomous medium-voltage converter-based microgrids with dynamic loads," *IEEE Transactions on Industrial Electronics*, vol. 61, no. 4, pp. 1643–1658, April 2014.

[6] A. Firdaus and S. Mishra, "Mitigation of power and frequency instability to improve load sharing among distributed inverters in microgrid systems," *IEEE Systems Journal*, pp. 1–10, 2019.

[7] A. Trivedi and M. Singh, "l_1 adaptive droop control for ac microgrid with small mesh network," *IEEE Transactions on Industrial Electronics*, vol. 65, no. 6, pp. 4781–4789, June 2018.

[8] X. Guo, Z. Lu, B. Wang, X. Sun, L. Wang, and J. M. Guerrero, "Dynamic phasors-based modeling and stability analysis of droop-controlled inverters for microgrid applications," *IEEE Transactions on Smart Grid*, vol. 5, no. 6, pp. 2980–2987, Nov 2014.

[9] D. K. Dheer, V. A. S, O. V. Kulkarni, and S. Doolla, "Improvement of stability margin of droop-based islanded microgrids by cascading of lead compensators," *IEEE Transactions on Industry Applications*, vol. 55, no. 3, pp. 3241–3251, May 2019.

[10] J. Condren and T. W. Gedra, "Expected-security-cost optimal power flow with small-signal stability constraints," *IEEE Transactions on Power Systems*, vol. 21, no. 4, pp. 1736–1743, Nov 2006.

[11] R. Zarate-Minano, F. Milano, and A. J. Conejo, "An opf methodology to ensure small-signal stability," *IEEE Transactions on Power Systems*, vol. 26, no. 3, pp. 1050–1061, Aug 2011.

[12] P. Li, H. Wei, B. Li, and Y. Yang, "Eigenvalue-optimisation-based optimal power flow with small-signal stability constraints," *IET Generation, Transmission Distribution*, vol. 7, no. 5, pp. 440–450, May 2013.

[13] P. Li, J. Qi, J. Wang, H. Wei, X. Bai, and F. Qiu, "An sqp method combined with gradient sampling for small-signal stability constrained opf," *IEEE Transactions on Power Systems*, vol. 32, no. 3, pp. 2372–2381, May 2017.

[14] Y. Li, G. Geng, Q. Jiang, W. Li, and X. Shi, "A sequential approach for small signal stability enhancement with optimizing generation cost," *IEEE Transactions on Power Systems*, vol. 34, no. 6, pp. 4828–4836, Nov 2019.

[15] P. Pareek and H. D. Nguyen, "Small-signal stability constrained optimal power flow: A convexification approach," 2019. [Online]. Available: https://arxiv.org/abs/1911.12001

[16] L. Luo and S. V. Dhople, "Spatiotemporal model reduction of inverter-based islanded microgrids," *IEEE Transactions on Energy Conversion*, vol. 29, no. 4, pp. 823–832, Dec 2014.

[17] http://www.penopt.com/penbmi.html, accessed: 2020-05-21.

[18] K. Michal and S. Michael, *PENNON: Software for Linear and Nonlinear Matrix Inequalities*. Boston, MA: Springer US, 2012, pp. 755–791.

[19] M. Kheirandishfard, F. Zohrizadeh, and R. Madani, "Convex relaxation of bilinear matrix inequalities part i: Theoretical results," in *2018 IEEE Conference on Decision and Control (CDC)*, Dec 2018, pp. 67–74.

[20] M. Kheirandishfard, F. Zohrizadeh, M. Adil, and R. Madani, "Convex relaxation of bilinear matrix inequalities part ii: Applications to optimal control synthesis," in *2018 IEEE Conference on Decision and Control (CDC)*, Dec 2018, pp. 75–82.

[21] X. Wu, C. Shen, and R. Iravani, "A distributed, cooperative frequency and voltage control for microgrids," *IEEE Transactions on Smart Grid*, vol. 9, no. 4, pp. 2764–2776, 2018.

[22] G. Chen and E. Feng, "Distributed secondary control and optimal power sharing in microgrids," *IEEE/CAA Journal of Automatica Sinica*, vol. 2, no. 3, pp. 304–312, 2015.

[23] M. C. Chandorkar, D. M. Divan, and R. Adapa, "Control of parallel connected inverters in standalone ac supply systems," *IEEE Transactions on Industry Applications*, vol. 29, no. 1, pp. 136–143, 1993.

[24] S. Boyd, L. E. Ghaoui, E. Feron, and V. Balakrishnan, *Linear Matrix Inequalities in System and Control Theory*. Philadelphia, PA: Society for Industrial and Applied Mathematics, 1994.

[25] F. Mei and B. Pal, "Modal analysis of grid-connected doubly fed induction generators," *IEEE Transactions on Energy Conversion*, vol. 22, no. 3, pp. 728–736, Sep. 2007.

[26] F. Zohrizadeh, M. Kheirandishfard, E. Q. Jnr, and R. Madani, "Penalized parabolic relaxation for optimal power flow problem," in *2018 IEEE Conference on Decision and Control (CDC)*, Dec 2018, pp. 1616–1623.

[27] http://cvxr.com/cvx/doc/mosek.html, accessed: 2020-06-28.

[28] A. Bidram, A. Davoudi, F. L. Lewis, and J. M. Guerrero, "Distributed cooperative secondary control of microgrids using feedback linearization," *IEEE Transactions on Power Systems*, vol. 28, no. 3, pp. 3462–3470, Aug 2013.

[29] R. D. Zimmerman and C. E. Murillo Sanchez, *MATPOWER Optimal Scheduling Tool (MOST) User's Manual 1.0.2*, june 2019.

[30] N. Bottrell, M. Prodanovic, and T. C. Green, "Dynamic stability of a microgrid with an active load," *IEEE Transactions on Power Electronics*, vol. 28, no. 11, pp. 5107–5119, 2013.